Central Lancashire Online Knowledge (CLoK)

Title	Resveratrol prevents long-term structural hippocampal alterations and modulates interneuron organization in an animal model of ASD
Type	Article
URL	https://clok.uclan.ac.uk/39024/
DOI	https://doi.org/10.1016/j.brainres.2021.147593
Date	2021
Citation	Santos-Terra, Júlio, Deckmann, Iohanna, Schwingel, Gustavo Brum, Paz, André Vinicius Contri, Gama, Clarissa S, Bambini-Junior, Victorio, Fontes-Dutra, Mellanie and Gottfried, Carmem (2021) Resveratrol prevents long-term structural hippocampal alterations and modulates interneuron organization in an animal model of ASD. Brain research, 1768. p. 147593. ISSN 1872-6240
Creators	Santos-Terra, Júlio, Deckmann, Iohanna, Schwingel, Gustavo Brum, Paz, André Vinicius Contri, Gama, Clarissa S, Bambini-Junior, Victorio, Fontes-Dutra, Mellanie and Gottfried, Carmem

It is advisable to refer to the publisher's version if you intend to cite from the work.
https://doi.org/10.1016/j.brainres.2021.147593

For information about Research at UCLan please go to http://www.uclan.ac.uk/research/

Brain Research

Resveratrol prevents long-term structural hippocampal alterations and modulates interneuron organization in an animal model of ASD
--Manuscript Draft--

Manuscript Number:	BRAINRES-D-21-00351R3
Article Type:	Research paper
Section/Category:	Cellular Neurobiology/Physiology
Keywords:	Autism Spectrum Disorder; resveratrol; animal model; hippocampus; interneuron; long-term alterations
Corresponding Author:	Júlio Santos-Terra, B.Sc. in Biomedical Sciences UFRGS: Universidade Federal do Rio Grande do Sul BRAZIL
First Author:	Júlio Santos-Terra, B.Sc. in Biomedical Sciences
Order of Authors:	Júlio Santos-Terra, B.Sc. in Biomedical Sciences
	Deckmann Iohanna, MSc
	Gustavo Brum Schwingel, MSc
	André Vinícius Contri Paz, MSc
	Clarissa Severino Gama, PhD
	Victorio Bambini-Junior, PhD
	Mellanie Fontes-Dutra, PhD
	Carmem Gottfried, PhD
Manuscript Region of Origin:	BRAZIL
Abstract:	Autism Spectrum Disorder (ASD) is a neurodevelopmental disorder characterized by impairments in both communication and social interaction, besides repetitive or stereotyped behavior. Although the etiology is unknown, environmental factors such as valproic acid (VPA) increase the risk of ASD onset. Resveratrol (RSV), a neuroprotective molecule, has been shown to counteract the effects of intrauterine exposure to VPA. We aimed to evaluate histological parameters related to hippocampal morphology and to the distribution of parvalbumin- (PV), calbindin- (CB), and somatostatin-positive (SOM) interneurons sub-populations, in addition to evaluate the total/phosphorylation levels of PTEN, AKT, GSK3β and total CK2 in the animal model of autism induced by VPA, as well as addressing the potential protective effect of RSV. On postnatal day 120, histological analysis showed a loss in total neurons in the dentate gyrus (DG) and decreased CB+ neurons in DG and CA1 in VPA animals, both prevented by RSV. In addition, PV+ neurons were diminished in CA1, CA2, and CA3, and SOM+ were interestingly increased in DG (prevented by RSV) and decreased in CA1 and CA2. A hippocampal lesion similar to sclerosis was also observed in the samples from the VPA group. Besides that, VPA reduced AKT and PTEN immunocontent, and both VPA and RSV increased CK2 immunocontent. Thus, this work demonstrated long-term effects of prenatal exposure to ASD in different sub-populations of interneurons, structural damage of hippocampus, and also alteration in proteins associated with pivotal cell signaling pathways, highlighting the role of RSV as a tool for understanding the pathophysiology of ASD.

Resveratrol prevents long-term structural hippocampal alterations and modulates interneuron organization in an animal model of ASD

Júlio Santos-Terra[#,1,2,3,4], Iohanna Deckmann[1,2,3,4], Gustavo Brum Schwingel[1,2,3,4], André Vinicius Contri Paz[5], Clarissa S. Gama[3,5,6], Victorio Bambini-Junior[1,3,4,7], Mellanie Fontes-Dutra[1,2,3,4], Carmem Gottfried[#,1,2,3,4]

1. Translational Research Group in Autism Spectrum Disorders-GETTEA, Universidade Federal do Rio Grande do Sul (UFRGS), Porto Alegre, RS, Brazil.
2. Department of Biochemistry, Universidade Federal do Rio Grande do Sul (UFRGS), Porto Alegre, RS, Brazil
3. National Institute of Science and Technology on Neuroimmunomodulation (INCT-NIM) - Brazil
4. Autism Wellbeing And Research Development (AWARD) Institute, BR-UK-CA
5. Laboratory of Molecular Psychiatry, National Science and Technology Institute for Translational Medicine, Hospital de Clínicas de Porto Alegre, Universidade Federal do Rio Grande do Sul (UFRGS), Brazil
6. Postgraduate Program in Psychiatry and Behavioral Sciences, Universidade Federal do Rio Grande do Sul (UFRGS), Porto Alegre, Brazil.
7. School of Pharmacology and Biomedical Sciences, University of Central Lancashire, Preston, United Kingdom

#CORRESPONDING AUTHORS:

JS-T (juliosterra@gmail.com) and CG (cgottfried@ufrgs.br)

Departamento de Bioquímica, ICBS, Universidade Federal do Rio Grande do Sul, Ramiro Barcelos 2600 – 21111. CEP: 90035-003 Porto Alegre-RS, Brazil.

E-MAIL ADDRESS OF EACH AUTHOR

JS-T (juliosterra@gmail.com)

ID (iohanna.deckmann@gmail.com)

GBS (brumschwingel@gmail.com)

AVCP (andrecontri@hotmail.com)

CSG (clarissasgama@gmail.com)

VB-J (VBambini-Junior@uclan.ac.uk)

MF-D (dutra.mellanie@gmail.com)

CG (cgottfried@ufrgs.br)

Highlights

Resveratrol prevents long-term structural hippocampal alterations and modulates interneuron organization in an animal model of ASD

Júlio Santos-Terra[#,1,2,3,4], Iohanna Deckmann[1,2,3,4], Gustavo Brum Schwingel[1,2,3,4], André Vinicius Contri Paz[5], Clarissa S. Gama[3,5,6], Victorio Bambini-Junior[1,3,4,7], Mellanie Fontes- Dutra[1,2,3,4], Carmem Gottfried[#,1,2,3,4]

1. Translational Research Group in Autism Spectrum Disorders-GETTEA, Universidade Federal do Rio Grande do Sul (UFRGS), Porto Alegre, RS, Brazil.
2. Department of Biochemistry, Universidade Federal do Rio Grande do Sul (UFRGS), Porto Alegre, RS, Brazil
3. National Institute of Science and Technology on Neuroimmunomodulation (INCT-NIM) - Brazil
4. Autism Wellbeing And Research Development (AWARD) Institute, BR-UK-CA
5. Laboratory of Molecular Psychiatry, National Science and Technology Institute for Translational Medicine, Hospital de Clínicas de Porto Alegre, Universidade Federal do Rio Grande do Sul (UFRGS), Brazil
6. Postgraduate Program in Psychiatry and Behavioral Sciences, Universidade Federal do Rio Grande do Sul (UFRGS), Porto Alegre, Brazil.
7. School of Pharmacology and Biomedical Sciences, University of Central Lancashire, Preston, United Kingdom

#CORRESPONDING AUTHORS:

JS-T (juliosterra@gmail.com) and CG (cgottfried@ufrgs.br)

Departamento de Bioquímica, ICBS, Universidade Federal do Rio Grande do Sul, Ramiro Barcelos 2600 – 21111. CEP: 90035-003 Porto Alegre-RS, Brazil.

HIGHLIGHTS

- Resveratrol prevents hippocampal morphological alterations induced by valproic acid;
- Resveratrol prevents alterations induced by valproic acid in interneurons;
- Valproic acid impairs protein expression associated with cell signaling pathways;
- Identification of long-term alterations may optimize the understanding of ASD.

Resveratrol prevents long-term structural hippocampal alterations and modulates interneuron organization in an animal model of ASD

Júlio Santos-Terra[#1,2,3,4], Iohanna Deckmann[1,2,3,4], Gustavo Brum Schwingel[1,2,3,4], André Vinicius Contri Paz[5], Clarissa S. Gama[3,5,6], Victorio Bambini-Junior[1,3,4,7], Mellanie Fontes-Dutra[1,2,3,4], Carmem Gottfried[#1,2,3,4]

1. Translational Research Group in Autism Spectrum Disorders-GETTEA, Universidade Federal do Rio Grande do Sul (UFRGS), Porto Alegre, RS, Brazil.
2. Department of Biochemistry, Universidade Federal do Rio Grande do Sul (UFRGS), Porto Alegre, RS, Brazil
3. National Institute of Science and Technology on Neuroimmunomodulation (INCT-NIM) - Brazil
4. Autism Wellbeing And Research Development (AWARD) Institute, BR-UK-CA
5. Laboratory of Molecular Psychiatry, National Science and Technology Institute for Translational Medicine, Hospital de Clínicas de Porto Alegre, Universidade Federal do Rio Grande do Sul (UFRGS), Brazil
6. Postgraduate Program in Psychiatry and Behavioral Sciences, Universidade Federal do Rio Grande do Sul (UFRGS), Porto Alegre, Brazil.
7. School of Pharmacology and Biomedical Sciences, University of Central Lancashire, Preston, United Kingdom

#CORRESPONDING AUTHORS:

JS-T (juliosterra@gmail.com) and CG (cgottfried@ufrgs.br)

Departamento de Bioquímica, ICBS, Universidade Federal do Rio Grande do Sul, Ramiro Barcelos 2600 – 21111. CEP: 90035-003 Porto Alegre-RS, Brazil.

E-MAIL ADDRESS OF EACH AUTHOR

JS-T (juliosterra@gmail.com)

ID (iohanna.deckmann@gmail.com)

GBS (brumschwingel@gmail.com)

AVCP (andrecontri@hotmail.com)

CSG (clarissasgama@gmail.com)

VB-J (VBambini-Junior@uclan.ac.uk)

MF-D (dutra.mellanie@gmail.com)

CG (cgottfried@ufrgs.br)

Abbreviations: AKT: AKT serine/threonine kinase 1; ASD: Autism Spectrum Disorder; CA 1-3: cornu ammonis (1-3); CB: calbindin; CK2: casein kinase 2; CNS: central nervous system; DG: dentate gyrus; GSK3β: glycogen synthase kinase 3 beta; HC: hippocampus; KO: knockout; mTOR: mechanistic target of rapamycin kinase; PTEN: phosphatase and tensin homologue; PV: parvalbumin; RSV: resveratrol; SOM: somatostatin; VPA: valproic acid.

ABSTRACT

Autism Spectrum Disorder (ASD) is a neurodevelopmental disorder characterized by impairments in both communication and social interaction, besides repetitive or stereotyped behavior. Although the etiology is unknown, environmental factors such as valproic acid (VPA) increase the risk of ASD onset. Resveratrol (RSV), a neuroprotective molecule, has been shown to counteract the effects of intrauterine exposure to VPA. We aimed to evaluate histological parameters related to hippocampal morphology and to the distribution of parvalbumin- (PV), calbindin- (CB), and somatostatin-positive (SOM) interneurons sub-populations, in addition to evaluate the total/phosphorylation levels of PTEN, AKT, GSK3β and total CK2 in the animal model of autism induced by VPA, as well as addressing the potential protective effect of RSV. On postnatal day 120, histological analysis showed a loss in total neurons in the dentate gyrus (DG) and decreased CB+ neurons in DG and CA1 in VPA animals, both prevented by RSV. In addition, PV+ neurons were diminished in CA1, CA2, and CA3, and SOM$^+$ were interestingly increased in DG (prevented by RSV) and decreased in CA1 and CA2. A hippocampal lesion similar to sclerosis was also observed in the samples from the VPA group. Besides that, VPA reduced AKT and PTEN immunocontent, and both VPA and RSV increased CK2 immunocontent. Thus, this work demonstrated long-term effects of prenatal exposure to ASD in different sub-populations of interneurons, structural damage of hippocampus, and also alteration in proteins associated with pivotal cell signaling pathways, highlighting the role of RSV as a tool for understanding the pathophysiology of ASD.

Keywords: Autism Spectrum Disorder, resveratrol, animal model, hippocampus, interneuron, long-term alterations.

1. INTRODUCTION

Autism Spectrum Disorder (ASD) is a highly prevalent neurodevelopmental disorder - affecting 1:54 children in the USA, the ratio of 4.3 boys to 1 girl (Maenner et al., 2020) - characterized by impairments in communication and social interaction, as well as repetitive and stereotyped behaviors (American Psychiatric Association, 2013). Despite extensive studies, the etiology of ASD remains unclear; however, it is already known that the final phenotype depends on the interaction between genetic and environmental risk factors (Gottfried et al., 2015). Among the environmental risk factors, the use of the anticonvulsant and mood stabilizer valproic acid (VPA) during pregnancy stands out (Dietert et al., 2011).

In addition to the main characteristics of this disorder, electrophysiological changes are also commonly described, including an imbalance in the delicate excitatory-inhibitory ratio (E/I) in different brain structures (Nelson and Valakh, 2015; Dickinson et al., 2016; Sohal and Rubenstein, 2019; Bruining et al., 2020). The dysfunctional predominance of glutamatergic action over GABAergic is one of the most frequent hypotheses to explain the E/I alterations (Marín and Rubenstein, 2003; Yizhar et al., 2011; Selten et al., 2018) in the central nervous system (CNS).

Interneurons promote the organization of circuits associated with cortical minicolumns and integrate stimuli among different cortical and subcortical regions. Within the subpopulations of these cells, parvalbumin (PV+) and somatostatin (SOM+) positive cells stand out as the most predominant (constituting about 70% of interneurons), in addition to other smaller subpopulations such as calbindin positive (CB+) (Kelsom and Lu, 2013).

In ASD patients, there are descriptions of reduction in PV+ neurons in the prefrontal cortex (Hashemi et al., 2017), while CB+ neurons have increased density in the dentate gyrus (DG) (Lawrence et al., 2010), but there are no findings describing SOM+ alterations. Deficits in PV+ interneurons have already been observed in the cortex of mice with *Mecp2* gene deletion, in the parietal cortex of animals from the VPA model (Gogolla et al., 2009), and in the prefrontal cortex of animals from the maternal immune activation model (Meyer et al., 2008). Regarding SOM+ interneurons, there are only descriptions of disorders associated with ASD.

The hippocampus (HC), a brain structure closely associated with memory, also contributes to several other behavior components, including sociability, flexible cognition (Rubin et al., 2014), and attention (Goldfarb et al., 2016). Interestingly, interneurons are fundamental to perform these functions: SOM+ interneurons are instrumental in keeping hippocampal synchrony, promoting electrophysiological balance and connectivity (Flossmann et al., 2019)/, while PV+ interneurons of ventral HC displayed important function

in social memory and social novelty recognition (Deng et al., 2019). Deficits in signaling mechanisms can also contribute to HC dysfunction, for example, the loss of PTEN in neurons of the DG induced increased excitability and connectivity (Santos et al., 2017; Skelton et al., 2019) and the hyperactivity of AKT-mTOR in the HC was associated with ASD-like behaviors (Xing et al., 2019).

Besides that, biological pathways associated with neural plasticity (CHU et al., 2013; WEI; HAN; ZHAO, 2020), such as AKT/GSK3β and CK2/PTEN, likewise can modulate interneurons. Loss of AKT signaling in cortical interneurons was already associated with reduced cell number (Carriere et al., 2020) whereas inhibition of AKT reduced the number of PV$^+$ cells in the HC (Chang et al., 2016). Studies suggest that GSK3β activity can be modulated by prenatal exposure to VPA (Caracci et al., 2016; Go et al., 2012; Wu et al., 2017) and, interestingly, the inhibition of AKT/GSK3β induced apoptosis of immature interneurons, leading to cell loss (Wei et al., 2020). The phosphatase and tensin homolog (PTEN) conditional knockout (KO) mice present ASD-like behavior and morphological neuronal changes (Cupolillo et al., 2016; Lugo et al., 2014; Shin et al., 2021), besides changes in the composition of interneuronal subpopulations, increasing PV$^+$ in detriment of SOM$^+$ (Vogt et al., 2015). Moreover, the specific KO of PTEN in both PV$^+$ and SOM+ induced ASD-like behavior (Shin et al., 2021). The casein kinase 2 (CK2) is a serine-threonine kinase protein that inactivates PTEN by phosphorylation (Borgo and Ruzzene, 2019). No evidence of a direct CK2 role in interneurons was already described; however, this protein already demonstrated important roles in the HC GABAergic signaling (Kim et al., 2020; Qin et al., 2021).

Recently, neuroimmune aspects have been largely associated with various disorders, including ASD (Gottfried et al., 2015). In this context, arises the resveratrol (RSV), a polyphenol widely studied in different diseases such as cancer, cardiovascular disorders, and diabetes due to its antioxidant and anti-inflammatory effect (Berman et al., 2017). Besides, RSV prevented behavioral and molecular changes in the VPA model, which has marked pro-oxidant and pro-inflammatory characteristics (Bambini-Junior et al., 2014; Fontes-Dutra et al., 2018; Hirsch et al., 2018). Thus, RSV emerges as an important method for assessing neuroimmune changes through its potential neuroprotective effect.

Here, we aimed to evaluate histological parameters related to hippocampal morphology and to the distribution of PV$^+$, SOM$^+$, and CB$^+$ interneurons sub-populations, in addition to evaluate the total/phosphorylation levels of PTEN, AKT, GSK3β, and CK2 in the animal model of autism induced by VPA, as well as assessing the potential protective effect of RSV.

2. RESULTS

2.1. Intrauterine administration of RSV prevented hippocampal long-term structural alterations in the VPA animals.

Prenatal exposure to VPA induced substantial structural alterations in the HC of adult animals (Figure 1B), leading to a discontinuity of the granule cell layer in the DG (Figure 1C) and a loss of neuronal compaction in the CA1 (Figure 1D). RSV entirely prevented the impact of VPA on these parameters.

2.2. Intrauterine administration of RSV prevented the long-term neuronal loss in the dentate gyrus of the VPA group.

RSV treatment prevented the decrease in the number of total neurons in the DG present in animals prenatally exposed to VPA ($F(1, 11) = 11.59$, p interaction = 0.0059, Figure 2A). No significant differences were observed in the CA1 (Figure 2B), CA2 (Figure 2C), and CA3 (Figure 2D) subregions. All neuron counts were normalized by area. Supplementary Table 1 comprises all means, standard deviation, and detailed statistics.

2.3. Intrauterine administration of RSV prevented long-term CB$^+$ and SOM$^+$ interneuron alterations in the dentate gyrus induced by prenatal exposure to VPA.

Regarding specific interneuron subpopulations, RSV treatment prevented the decrease in the number of CB$^+$ Neurons/Area induced by prenatal exposure to VPA ($F(1,10) = 12.43$; p interaction = 0.0055, Figure 3A1). No differences were seen in CB$^+$ Ratio/Total Neurons (Figure 3A2). In addition, no significant differences were observed in either PV$^+$ Neurons/Area (Figure 3B1) or PV$^+$ Ratio/Total Neurons (Figure 3B2).

Interestingly, significant differences were observed in both factors separately ($F(1,11) = 11.03$, p RSV <0.0001; $F(1,11) = 45,52$, p VPA <0.0001) in SOM$^+$ Neurons/Area (Figure 3C1). RSV prevented the increase in SOM$^+$ Ratio/Total Neurons induced by prenatal exposure to VPA ($F(1,11) = 8.821$; p interaction= 0.0127, Figure 3C2).

The illustrative Figure 3 shows CB$^+$ neurons (Figure 3A), PV$^+$ neurons (Figure 3B), and SOM$^+$ neurons (Figure 3C) in the DG. All neuron counts were normalized by area. Supplementary Tables 2, 3, and 4 comprise all means, standard deviation, and detailed statistics for CB$^+$, PV$^+$, and SOM$^+$ interneurons, respectively.

2.4. Intrauterine exposure to VPA induced long-term alterations in CB⁺, PV⁺, and SOM⁺ interneurons parameters in the CA1 subregion, whilst RSV prevented CB⁺ and PV⁺ parameters, as well as demonstrated a *per se* effect in SOM⁺.

RSV prenatal treatment prevented both the decrease in CB⁺ Neurons/Area ($F_{(1,10)}$ = 27.50, p interaction = 0.0004, Figure 4A1) and CB⁺ Ratio/Total Neurons induced by prenatal exposure to VPA ($F_{(1,10)}$ = 11.52; p interaction = 0.0068, Figure 4A2).

Again, the prenatal exposure to VPA modified interneuron subpopulations in this subregion, decreasing the PV⁺ Neurons/Area ($F_{(1,12)}$ = 8.261; p interaction = 0.0140, Figure 4B1). Besides, a decrease in PV⁺ Ratio/Total Neurons was observed in both groups exposed to VPA with no RSV preventive effects ($F_{(1, 12)}$ = 7.634, p VPA = 0.0172, Figure 4B2).

No differences were seen in SOM⁺ Neurons/Area (Figure 4C1). Considering SOM⁺ Ratio/Total Neurons, significant differences were seen in the factors separately ($F_{(1,11)}$ = 12.79, p RSV = 0.0043; $F_{(1,11)}$ = 7.953, p VPA = 0.0167): both prenatal exposure to VPA and treatment with RSV (including *per se* effect) decreased SOM⁺ Ratio/Total Neurons (Figure 4C2).

The illustrative Figure 4 shows CB⁺ neurons (Figure 4A), PV⁺ neurons (Figure 4B), and SOM⁺ neurons (Figure 4C) in the CA1. All neuron counts were normalized by area. Supplementary Tables 2, 3, and 4 comprise all means, standard deviation, and detailed statistics for CB⁺, PV⁺, and SOM⁺ interneurons, respectively.

2.5. Intrauterine exposure to VPA induced long-term alterations in SOM⁺ and PV⁺ interneurons parameters in the CA2 subregion, without preventive effect of RSV.

No significant differences were found in either CB⁺ Neurons/Area (Figure 5A1) or CB⁺ Ratio/Total Neurons (Figure 5A2) among groups, as well as PV⁺ Neurons/Area (Figure 5B1). However, the VPA administration during pregnancy decreased PV⁺ Ratio/Total Neurons ($F_{(1,12)}$ = 7.043; p VPA = 0.0210) without RSV prevention (Figure 5B2).

Regarding SOM⁺, there was a significant difference only in the effect of VPA ($F_{(1,11)}$ = 7.172, p VPA = 0.0215), decreasing SOM⁺ Neurons/Area in comparison to groups not exposed to VPA (Figure 5C1). Besides that, RSV treatment prevented the decrease in SOM⁺ Ratio/Total Neurons induced by prenatal exposure to VPA ($F_{(1,11)}$ = 18.54; p interaction = 0.0012, Figure 5C2).

The illustrative Figure 5 shows CB⁺ neurons (Figure 5A), PV⁺ neurons (Figure 5B), and SOM⁺ neurons (Figure 5C) in the CA2. All neuron counts were normalized by area. Supplementary Tables 2, 3, and 4 comprise all means, standard deviation, and detailed statistics for CB⁺, PV⁺, and SOM⁺ interneurons, respectively.

2.6. Intrauterine exposure to VPA induced long-term alteration in PV$^+$ interneurons parameters in the CA3 subregion, without preventive effect of RSV.

No significant differences were found in either CB$^+$ Neurons/Area (Figure 6A1) or CB$^+$ Ratio/Total Neurons (Figure 6A2) among groups.

Regarding PV$^+$, prenatal exposure to VPA decreased both PV$^+$ Neurons/Area (F(1,12) = 8.859, p interaction = 0.0116, Figure 6B1) and PV$^+$ Ratio (F(1,12) = 11.56, p interaction = 0.0012, Figure 6B2).

Lastly, no significant differences were found in either SOM$^+$ Neurons/Area (Figure 6C1) or SOM$^+$ Ratio/Total Neurons (Figure 6C2) among groups.

The illustrative Figure 6 shows CB$^+$ neurons (Figure 6A), PV$^+$ neurons (Figure 6B), and SOM$^+$ neurons (Figure 6C) in the CA3. All neuron counts were normalized by area. Supplementary Tables 2, 3, and 4 comprise all means, standard deviation, and detailed statistics for CB$^+$, PV$^+$, and SOM$^+$ interneurons, respectively.

2.7. VPA induced long-term alterations in the hippocampal immunocontents of AKT, PTEN, and CK2 without preventive effect of RSV.

The animals prenatally exposed to VPA (VPA and VPA+RSV) presented decreased levels of PTEN when compared to the other groups (Control and RSV) (F(1,20) = 21.22; p VPA = 0.0002) (Supplementary Table 5, Figure 7A).

There were significant differences in RSV factor (F(1,19) = 4.406; p RSV = 0.0494) and VPA factor (F(1,19) = 10.64, p VPA = 0.0041) in the AKT immunocontent, indicating a decrease in the total AKT levels induced by VPA when compared to the Control group with no preventive effect of RSV treatment (Supplementary Table 5, Figure 7B).

In addition, prenatal exposure to VPA increased the total CK2 immunocontent (F(1,20) = 6.628, p = 0.0181) without RSV preventive effect (Supplementary Table 5, Figure 7C).

Finally, no changes were observed in the GSK3β immunocontent (Supplementary Table 4, Figure 7D) and in the phosphorylation levels of the proteins among groups (Supplementary Table 5). Supplementary Figures 1, 2, and 3 represent the nitrocellulose membranes stained with ponceau, as well as images of immunoblottings of the specific primary antibodies, and of the endogenous marker β-actin, respectively.

3. DISCUSSION

Considering that most studies investigate behavioral and morphological alterations in young animals, we set out to evaluate possible changes in the adults of the ASD model induced by prenatal exposure to VPA. Several studies have been focused on the HC due to its plasticity and sensitivity to stressors, in addition to being an area where neurogenesis occurs in adulthood, both in rodents and in humans (Gonçalves et al., 2016). Our research group previously demonstrated age-dependent alterations in the HC of the VPA animal model regarding glutamate metabolism at P15 and P120 (Bristot Silvestrin et al., 2013). At P15, the VPA animals had decreased levels of glutamate transporter GLT1 and increased levels of glutamine synthetase (GS). At P120, the VPA animals had increased glutamate uptake activity, increased levels of GLT1, increased levels of glutathione (GSH), and decreased activity of GS. These data demonstrate important glutamatergic alterations in HC, probably associated with a glutamatergic excitotoxicity pattern already demonstrated in ASD.

In the present study, we demonstrated a significant morphological alteration in hippocampal regions induced by VPA in adult animals at P120. The altered cellular composition in the model of ASD is most prominent in DG, particularly in the granular layer. Moreover, neurons appeared dispersed in CA1. Interestingly, RSV prevented these alterations, indicating some of the preventive behavioral effects observed in previous works (Bambini-Junior et al., 2014; Fontes-Dutra et al., 2018; Hirsch et al., 2018) might be related to direct effects in the HC.

Studies demonstrated the benefits of RSV in restoring hippocampal structure and connectivity in patients with mild cognitive impairments (Köbe et al., 2017) and status epilepticus (Castro et al., 2017), although no significant effects were observed in behavioral tasks of memory performance. These findings might suggest possible similar mechanisms since our previous data revealed no significant effects of RSV in empathy-like prosocial behavior in RSV+VPA rats of similar age (Fontes-Dutra et al., 2019).

The mechanisms of RSV protection are not well established, but some hypotheses grow towards the action of RSV in activating SIRT proteins, especially in view of the HDAC inhibitor action associated with VPA. The hippocampal activity of SIRT1 is fundamental for cognition, memory and synaptic plasticity (Castrol et al., 2017); a study demonstrated that miR-134 mediates these functions through CREB (Gao et al., 2010) and, interestingly, we already demonstrated that RSV normalized the altered levels of mir-134 induced by VPA in our model (Hirsch et al., 2018). Finally, SIRT1 stimulation of mitochondrial biogenesis and activity (mediated by PGC-1α) protected the HC from seizure-induced cell death and reduced oxidative stress (Wang et al., 2015; Chuang et al., 2019), indicating another possible pathway by which RSV plays neuroprotective effects.

Hippocampal excitotoxicity has been associated with neuropsychiatric disorders (Olloquequi et al., 2018), such as ASD (Essa et al., 2013), schizophrenia (Plitman et al., 2014), epilepsy (Thom, 2014), and many others. In schizophrenia, an altered organization in the granular layer from DG is observed in GFAP.HMOX10-12m transgenic model, which astrocytes overexpress the human stress protein heme oxygenase-1 (OX1) (Tavitian et al., 2019), leading to an "immature" DG associated with changes in its molecular profile. In epilepsy, age-dependent patterns of DG are observed, such as neuronal loss in granular cells and CA1 (Pauli et al., 2006; Thom, 2014). These changes in hippocampal structure and shape are relevant to establish the histological hallmarks of hippocampal sclerosis, which involves a neuronal loss in hippocampal subregions, gliosis, or both of them in different levels (Thom, 2014). The present findings suggest possible mechanisms related to this event, opening an interesting issue to be followed up to characterize glial cell alteration in adult VPA rats.

Hippocampal interneurons are a highly diverse population of cells, with functions associated with shape, neurochemical patterns, and location (Maccaferri and Lacaille, 2003). The evaluation of HC subregions CA1, CA2, CA3, and DG at P120 indicated an expansion of the damage induced by prenatal exposure to VPA. In addition to the morphological alteration, also decreased total neurons of DG associated with different natures of alteration among CB$^+$, PV$^+$ and SOM$^+$ interneuronal subpopulations.

In DG, VPA reduced the number and the ratio of CB$^+$ interneurons, which was prevented by RSV treatment. CB$^+$ interneurons in DG already demonstrated to be influenced by the electrophysiological status: hippocampal epilepsy in humans induced morphological impairments on CB$^+$ interneurons both hypertrophy of cell bodies and spiny dendrites (Maglóczky et al., 2000), and loss of general calbindin expression in this region (Bandopadhyay et al., 2014), although, in ASD, a previous study demonstrated increased density of CB$^+$ interneurons in DG (Lawrence et al., 2010). Interestingly, in a schizophrenia animal model, rats demonstrated an important reduction of CB$^+$ interneurons in DG (Harte et al., 2007); complementarily, a recent study demonstrated the critical role of DG CCK$^+$ interneurons (which are mostly CB$^+$) (Pelkey et al., 2017) in the inhibitory plasticity processes associated with the promotion of enriched early social, sensory and motor experiences (Feng et al., 2020). Furthermore, our group demonstrated that RSV improved early sensory alterations (Fontes-Dutra et al., 2018) and social and stereotypy impairments (Bambini-Junior et al., 2014; Hirsch et al., 2018) possibly due to the protection of early loss of important experiences, preserving this component (CB$^+$/CCK$^+$) feature of HC inhibitory circuit.

SOM+ interneurons demonstrated a distinct pattern in DG, not only due to the total neuronal loss (which could increase the SOM$^+$/total neurons by itself) but also due to increased absolute neuronal numbers. The SOM$^+$ cells play important roles in DG, promoting contralateral HC connectivity (Eyre and Bartos, 2019), organizing granule cell assemblies associated with memory formation (Yuan et al., 2017) and regulating long term potentiation (Tallent, 2007). Little is known about SOM$^+$ interneurons in the ASD context. Previous work already demonstrated that the haploinsufficiency of Aridb1 (risk-associated gene for ASD) in SOM$^+$ cells induces stereotypies and learning/memory issues (Smith et al., 2020). In Dravet syndrome (which is significantly related to ASD behavioral features), SOM$^+$ cells presented reduced excitability (Chao Tai et al., 2014). Although SOM$^+$ and CB$^+$ cells have different embryonic origins (MGE and CGE, respectively) (Kelsom and Lu, 2013), one factor is pivotal to the final interneuron positioning in a specific region: the microenvironment during the moment of arrival. For SOM$^+$ cells, the present complementary changes in CA1 and CA2 subregions (both in number and ratio, with prevention by RSV only in the CA2 ratio and an including an apparent *per se* effect of RSV towards reduction of SOM ratio in CA1) indicate that VPA may interfere on migration routes, retaining SOM$^+$ neurons in DG. Impairments in CXCL12 signaling, for example, can misplace the interneurons distribution in HC. Indeed, VPA can interfere with CXCR4 (CXCL12 receptor) (Gul et al., 2009) and induce neuronal accumulation in DG, which replicates the SOM+ neurons pattern (Danzer, 2019). Thus, considering that CA1 and CA2 remain altered at some level in the VPA+RSV group, these changes are probably not related to the core symptoms of ASD.

Differently, RSV may be inducing important effects during pregnancy that prevent DG interneuron alterations, highlighting this subregion as a possible critical component in ASD. However, the *per se* effect of RSV in CA1 highlights the necessity to expand the understanding of the cellular pathways associated with the placement of interneurons in this particular subregion. Moreover, the preventive effect of RSV against VPA-induced total neurons decrease may possibly be related to glutamatergic signaling modulation, such as the AMPA signaling (Manent et al., 2006) and other pathways of signaling (Luhmann et al., 2015), providing important clues to support the correct interneuronal positioning in the RSV+VPA group.

In CA1, we observed important alterations among interneurons subpopulations induced by VPA, including a reduction in PV$^+$ number and SOM$^+$ cells. The prenatal administration of RSV was able to prevent CB$^+$ interneurons-decrease in number and ratio. PV$^+$ interneurons have been studied in neurodevelopmental context, description of impairments in several animal models includes the presence of ASD-like features in mice

KO for PV (PV$^{-/-}$) (Wöhr et al., 2015), downregulation of PV expression in Angelman Syndrome model (Godavarthi et al., 2014) and altered neuronal layer positioning (increased ratio in superficial layers II-III and reduction in deeper layers IV/V) in somatosensory cortex (Fontes-Dutra et al., 2018). Interestingly, PV$^+$ cells in CA1 presents important roles in memory consolidation (Ognjanovski et al., 2017), particularly social memory (Deng et al., 2019) and spatial working memory (Murray et al., 2011), indicating that impairments in this hippocampal subregion may contribute to the empathy-like behavioral alteration that we observed in ASD model. Interestingly, in CA2 and CA3, we also observed a similar pattern for PV$^+$ cells, which usually are associated with a complex synaptic organization and the generation of fast-ripples waves (Kohus et al., 2016; Sik et al., 1993), fundamental for memory, planning, and interactions with other regions like the prefrontal cortex (Buzsáki, 2015; Sullivan et al., 2011).

Related to the evaluated signaling pathways, we demonstrated that RSV could not prevent the hippocampal changes of total PTEN, CK2, and AKT. However, considering that no changes were observed in phosphorylation levels and consequently the activity of PTEN, AKT, and GSK3β among groups, it suggests that, at least in HC from P120 animals, these proteins might not play an important role in ASD-like features. PTEN KO mice in PV$^+$ and SOM$^+$ cells displayed social deficits, repetitive behaviors, and impaired motor coordination/learning similar to ASD. Besides, these animals presented interneuron-dependent behavior alterations: PTEN KO mice in SOM$^+$ displayed anxiety-like behaviors, while PTEN KO mice in PV+ presented hyperlocomotion (Shin et al., 2021). Furthermore, one of the proteins that regulate PTEN is CK2, which can inhibit PTEN activity. Here, we observed an increase in the levels of this protein, which confirms the decrease in PTEN also found. Finally, the decrease in AKT may impact mTOR activity which would, in turn, affect synaptic components (Nicolini et al., 2015). Therefore, even if the protein changes demonstrated here cannot fully explain the behavioral and morphological issues of the VPA model, its participation in the autistic phenotype remains to be determined in other brain structures and age.

In summary, the present data shed some light on the ASD pathophysiology at adult age, demonstrating long-term alterations of the gestational VPA-exposure in a key brain region implicated in the many impairments described in ASD, such as sociability and flexible cognition. Furthermore, the most widely available data refer to infant or juvenile ages; few studies focus on bringing insights to the progressive damage of ASD in adult stages, which enhances the translational character of our data as it provides evidence that can improve the understanding of the symptoms associated with ASD in adult patients. Moreover, the

alterations observed in the hippocampal morphology, neuronal composition, and expression of important signaling proteins contribute to the hypothesis of an E/I imbalance in ASD. Especially regarding SOM⁺ neurons, this is the first work to our knowledge to demonstrate the involvement of this interneuron in the VPA-ASD animal model, highlighting a new field of study in the disorder. Finally, we demonstrated a long-term preventive effect of prenatal treatment with RSV, being effective in adult ages, particularly related to changes in the neuronal composition of the dentate gyrus and in the morphology of the HC.

4. CONCLUSION

In summary, we demonstrated that prenatal exposure to VPA induced significant hippocampal alterations in morphology, neuronal composition, and protein expression in adult animals with significant preventive effects of RSV. These data highlight the long-term neuroprotection provided by this polyphenol, especially in DG. Considering that the timing of a risk factor exposure during pregnancy is pivotal for ASD triggering and development, with long-term impacts in the nervous system, preventive effects of RSV in HC open new clues in the understanding of ASD pathophysiology. However, the mechanisms behind this pattern are still open to study.

5. METHODOLOGY

5.1. Animals

Wistar rats from the Center for Reproduction and Experimentation of Laboratory Animals (CREAL) were housed in the bioterium of the Department of Biochemistry and maintained under a standard 12/12h light/dark cycle at a constant temperature of 22±2°C. The animals had *ad libitum* access to food and water and were handled following the guidelines established by the National Council for the Control of Animal Experimentation (CONCEA) of Brazil. The ethics committee approved this project of the Federal University of Rio Grande do Sul (CEUA-UFRGS #35733). The animals' euthanasia was performed by anesthetic overdose with ketamine and xilasine, supplied in concentrations three times higher than the concentration required to obtain an anesthetic-surgical plan (300 mg/kg and 40 mg/kg, respectively), following the Euthanasia Practice Guidelines of the National Council for Animal Experimentation Control (Normative Resolution N. 13, 2013).

5.2. Drugs and prenatal treatments

5.2.1. *Drugs*

For inducing the model and experimental treatments, we used resveratrol (RSV - 3.6 mg/Kg; Fluxome, Stenløse, Denmark), dimethyl sulfoxide (DMSO - P.A., equivalent volume of RSV injection; Merck, Germany), valproic acid (VPA - 600 mg/Kg; Acros Organics, NJ, USA).

5.2.2. *Prenatal treatments*

Males and females rats were mated overnight, and pregnancy was verified the next morning through the presence of spermatozoa in the vaginal smear; after pregnancy was confirmed, this day was considered the embryonic day 0.5 (E0.5). Pregnant rats were divided into four groups according to the treatment they received: Control (vehicles), RSV, VPA, or RSV+VPA. From E6.5 to E18.5, the pregnant rats received a daily subcutaneous injection of RSV (Fluxome, Stenløse, Denmark) at 3.6 mg/Kg or dimethyl sulfoxide P.A. (DMSO, equivalent volume of RSV injection) as previously described (Bambini-Junior et al., 2014; Fontes-Dutra et al., 2018). On E12.5, pregnant rats received a single intraperitoneal injection with either VPA at 600 mg/Kg (Acros Organics, NJ, USA) or saline solution 0.9%. Pregnant rats were isolated in E18 until the litter's birth. We consider the day of the birth the postnatal day 0 (P0). The female pups were euthanized at postnatal day (P) P21, and only males were used in this work. After birth and weaning at P21, male offspring were kept until P120. 3-4 animals from different litters per group were used for immunofluorescence assays, and 6 animals from different litters per group were used for western blotting assays. The sample number for the immunofluorescence assay was CON = 4, RSV = 4, VPA = 4 and RSV + VPA = 3; for western blotting, it was 6 for all experimental groups. The animals came from different litters. The total number of animals used in the study was 10 control, 10 RSV, 10 VPA, and 9 RSV+VPA divided randomly in experiments, generated from 6 control dams, 6 RSV, 12 VPA, and 12 RSV+VPA (the excedent offspring was destined to other projects in order to use of biological tissue). Loss rate for the VPA groups was 50% in this protocol.

5.3. Immunofluorescence

The tissues fixed and cryopreserved in OCT® were cut in a Leica® cryostat (-20ºC) and the slices (25 μm) corresponding to the HC were placed on histological slides covered with poly-L-lysine and post-fixed again with 4% paraformaldehyde. We intended to comprise within the following coordinates: bregma: -2.92 mm, interaural: 6.08 mm, Figure 57 in Paxinos Atlas (5th edition) - bregma: -3.24 mm, interaural: 5.76 mm, Figure 60 in Paxinos

Atlas (5th edition). In each histological slide, 3 slices were alternately placed. After that, the staining was performed using specific primary antibodies for PV, SOM, CB, and NeuN, in addition to corresponding secondary antibodies associated with a fluorophore (Alexia® 488 and Alexia® 594) and nuclear DAPI dye according to the protocol described by Fontes-Dutra et al., 2018. The analysis was performed in duplicates. Technical information, including concentrations of the reagents used in immunofluorescence assays, are summarized in Supplementary Table 6. The images were obtained using the Olympus FV1000® confocal microscope at the Center for Microscopy and Microanalysis (CMM-UFRGS) and the Nikon® E600 fluorescence microscope at the Department of Biochemistry (UFRGS). Each coronal section of 25 μm is photographed in stacks by the confocal microscope (on average, 8, dimensions: 635.9 x 635.9 microns). The analyses were performed using the ImageJ® software using the Cell Counter plug-in. The quantification was conducted by counting cells of the 8 stacks of at least 2 slices per animal (all the stacks individually and also with the overlapping image). The counting is done manually by two trained researchers, who are blinded for the experimental groups.

Quantitative evaluation was performed by the absolute number of total neurons (NeuN+) and interneurons (CB$^+$, PV$^+$, and SOM$^+$) - normalized by area - in addition to the ratio between the number of interneurons and total neurons to obtain a ratio between the inhibitory (interneuron) and excitatory components (the majority of the total neurons) according to the following formula: (CB$^+$, PV$^+$ or SOM$^+$) Interneurons/Total neurons (based on Fontes-Dutra et al., 2018). This ratio was made separately for each interneuron evaluated. These assessments were made in the dentate gyrus (DG), CA1, CA2, and CA3.

Due to the magnification used to capture the images (20x), one counting frame was obtained in each subfield (subregion) in each hemi-hippocampus. All images were obtained with a standardized size (635.9x635.9 μm^2) containing a representative portion of each subregion DG, CA1, CA2, and CA3. Considering the anatomical differences intrinsic to biological models, the quantification area of the subregion DG was determined by the contour of the granular layer whilst the contour of CA1/CA2/CA3 was defined as the delimitation of the pyramidal cells layer (Supplementary Figure 4). The averages of the areas in the subfields per animal were DG: 85,104±10,151 μm^2; CA1: 39,638±8,445 μm^2; CA2: 106,168±24,254 μm^2; CA3: 47,478±8,288 μm^2, the average of the total area analyzed per animal was 278,743±33,570 μm^2. All cells present within the delimited region (and the interneurons surrounding the pyramidal/granular layers) were quantified. The averages of the total neurons analyzed in the subfields per animal were DG: 582±64; CA1: 150±18; CA2: 265±42; CA3: 136±15, the average of the total neurons analyzed per animal was 1,113±93.

The averages of CB$^+$ neurons analyzed in the subfields per animal were DG: 6.5±1.6; CA1: 3.6±1.2; CA2: 6.7±2; CA3: 3.5±1, the average of CB$^+$ neurons per animal was 20.4±4.5. The averages of PV$^+$ neurons in the subfields per animal were DG: 12.5±2.3; CA1: 6.7±1.9; CA2: 10.6±1.9; CA3: 5.8±1.4, the average of PV$^+$ neurons per animal was 35.6±5.1. The averages of SOM$^+$ neurons in the subfields per animal were DG: 25±12.1; CA1: 5.5±1.79; CA2: 7.75±3.35; CA3: 4.75±1.2, the average of SOM$^+$ neurons per animal was 43.2±10.

5.4. Protein immunocontent by Western Blotting

The hippocampal samples were homogenized and prepared in a buffer containing 10% SDS, 100mM EDTA, 500mM TRIS, and protease inhibitor, centrifuged at 14000 g for 20 min at 4ºC, and the supernatant was collected. Total proteins were quantified by the Lowry method (LOWRY et al., 1951), samples were prepared in a buffer containing glycerol, bromophenol blue, and 500 mM TRIS, and β-mercaptoethanol. Equal amounts of protein (40µg) were applied to 12% polyacrylamide gels, separated by unidimensional electrophoresis and transferred to nitrocellulose membranes to detect the immunocontent of CK2, PTEN, p-PTEN (Ser380, Thr382/383), AKT, p-AKT (Ser473 and Thr380), GSK3β and p-GSK3β proteins using specific primary antibodies according to the protocol adapted from (Bristot Silvestrin et al., 2013) The analysis was performed in duplicates. After incubation with corresponding secondary peroxidase-associated antibodies (HRP), the chemiluminescent signal was detected using the ImageQuant™ LAS 4000 system (GE HealthCare Life Sciences®). The quantification of the relative immunocontent was performed with the ImageJ® software, and the data were normalized by the endogenous marker β-actin. Technical information, including concentrations of the reagents used in Western Blotting assays, are summarized in Supplementary Table 7.

5.5. Statistical analysis

The analysis was performed using the GraphPad Prism 6 software (GraphPad Software, La Jolla, California US). Kolmogorov-Smirnov and Shapiro-Wilk tests of normality were applied to determine data distribution. As the data presented a normal distribution, we chose a parametric test (two-way ANOVA) followed by Bonferroni post-test. When there was an interaction effect, pairwise comparison was analyzed in the post hoc; when there was no effect, exposure to factors (VPA or RSV) was analyzed.

6. AUTHOR CONTRIBUTIONS

JS-T, ID, GBS, MF-D, AVCP, CSG, VB-J, and CG: experimental design and intellectual contribution. CSG, VB-J, and CG: acquisition of financial resources. JS-T, ID, and MF-D: immunofluorescence analyses. JS-T, ID, AVCP, and GBS: western blotting analyses. JS-T, ID, MF-D, CSG, VB-J, and CG: data discussion and manuscript preparation.

7. ACKNOWLEDGEMENTS

8. CONFLICT OF INTEREST STATEMENT

The authors declare that the research was conducted in the absence of any commercial or financial relationships that could be considered a potential conflict of interest.

9. REFERENCES

American Psychiatric, 2013. DSM 5, American Journal of Psychiatry. https://doi.org/10.1176/appi.books.9780890425596.744053

Bambini-Junior, V., Zanatta, G., Della Flora Nunes, G., Mueller de Melo, G., Michels, M., Fontes-Dutra, M., Nogueira Freire, V., Riesgo, R., Gottfried, C., 2014. Resveratrol prevents social deficts in animal model of autism induced by valproic acid. Neurosci. Lett. 583, 176–181. https://doi.org/10.1016/j.neulet.2014.09.039

Bandopadhyay, R., Liu, J.Y.W., Sisodiya, S.M., Thom, M., 2014. A comparative study of the dentate gyrus in hippocampal sclerosis in epilepsy and dementia. Neuropathol. Appl. 40, 177-190. Neurobiol. https://doi.org/10.1111/nan.12087

Berman, A.Y., Motechin, R.A., Wiesenfeld, M.Y., Holz, M.K., 2017. The therapeutic

potential of resveratrol: a review of clinical trials. NPJ Precis. Oncol. 1. 1, 35. https://doi.org/10.1038/s41698-017-0038-6

Borgo, C., Ruzzene, M., 2019. Role of protein kinase CK2 in antitumor drug resistance. J. Exp. Clin. Cancer Res. 6, 138. https://doi.org/10.1186/s13046-019-1292-y

Bristot Silvestrin, R., Bambini-Junior, V., Galland, F., Daniele Bobermim, L., Quincozes-Santos, A., Torres Abib, R., Zanotto, C., Batassini, C., Brolese, G., Gonçalves, C.-A., Riesgo, R., Gottfried, C., 2013. Animal model of autism induced by prenatal exposure to valproate: Altered glutamate metabolism in the hippocampus. Brain Res. 1495, 52–60. https://doi.org/10.1016/j.brainres.2012.11.048

Bruining, H., Hardstone, R., Juarez-Martinez, E.L., Sprengers, J., Avramiea, A.-E., Simpraga, S., Houtman, S.J., Poil, S.-S., Dallares, E., Palva, S., Oranje, B., Palva, J.M., Mansvelder, H.D., Linkenkaer-Hansen, K., 2020. Measurement of excitation-inhibition ratio in autism spectrum disorder using critical brain dynamics. Sci. Reports 2020 101 10, 1–15. https://doi.org/10.1038/s41598-020-65500-4

Buzsáki, G., 2015. Hippocampal sharp wave-ripple: A cognitive biomarker for episodic memory and planning. Hippocampus 25(10), 1073-1188. https://doi.org/10.1002/hipo.22488

Caracci, M.O., Avila, M.E., De Ferrari, G. V., 2016. Synaptic Wnt/GSK3 β Signaling Hub in Autism. Neural Plast. 2016, 7149527. https://doi.org/10.1155/2016/9603751

Carriere, C.H., Wang, W.X., Sing, A.D., Fekete, A., Jones, B.E., Yee, Y., Ellegood, J., Maganti, H., Awofala, L., Marocha, J., Aziz, A., Wang, L.Y., Lerch, J.P., Lefebvre, J.L., 2020. The γ-protocadherins regulate the survival of GABAergic interneurons during developmental cell death. J. Neurosci. 40, 8652–8668. https://doi.org/10.1523/JNEUROSCI.1636-20.2020

Castro, O.W., Upadhya, D., Kodali, M., Shetty, A.K., 2017. Resveratrol for easing status epilepticus induced brain injury, inflammation, epileptogenesis, and cognitive and memory dysfunction-Are we there yet? Front. Neurol. 8, 603. https://doi.org/10.3389/fneur.2017.00603

Chang, C.Y., Chen, Y.W., Wang, T.W., Lai, W.S., 2016. Akting up in the GABA hypothesis of schizophrenia: Akt1 deficiency modulates GABAergic functions and hippocampus-

dependent functions. Sci. Rep. 6, 33095. https://doi.org/10.1038/srep33095

Chuang, Y.C., Chen, S. Der, Jou, S. Bin, Lin, T.K., Chen, S.F., Chen, N.C., Hsu, C.Y., 2019. Sirtuin 1 regulates mitochondrial biogenesis and provides an endogenous neuroprotective mechanism against seizure-induced neuronal cell death in the hippocampus following status epilepticus. Int. J. Mol. Sci. 20(14), 3588. https://doi.org/10.3390/ijms20143588

Cupolillo, D., Hoxha, E., Faralli, A., De Luca, A., Rossi, F., Tempia, F., Carulli, D., 2016. Autistic-like traits and cerebellar dysfunction in purkinje cell PTEN knock-out mice. Neuropsychopharmacology 41(6), 1457-1466. https://doi.org/10.1038/npp.2015.339

Danzer, S.C., 2019. Valproic Acid Leads New Neurons Down the Wrong Path. Epilepsy Curr. 19(2):132-133. https://doi.org/10.1177/1535759719835366

Deng, X., Gu, L., Sui, N., Guo, J., Liang, J., 2019. Parvalbumin interneuron in the ventral hippocampus functions as a discriminator in social memory. Proc. Natl. Acad. Sci. U. S. A. 116, 16583–16592. https://doi.org/10.1073/pnas.1819133116

Dickinson, A., Jones, M., Milne, E., 2016. Measuring neural excitation and inhibition in autism: Different approaches, different findings and different interpretations. Brain Res. 1648, 277–289. https://doi.org/10.1016/J.BRAINRES.2016.07.011

Dietert, R.R., Dietert, J.M., DeWitt, J.C., 2011. Environmental risk factors for autism. Emerg. Health Threats J. 4, 7111. https://doi.org/10.3402/ehtj.v4i0.7111

Endo, H., Nito, C., Kamada, H., Nishi, T., Chan, P.H., 2006. Activation of the Akt/GSK3β signaling pathway mediates survival of vulnerable hippocampal neurons after transient global cerebral ischemia in rats. J. Cereb. Blood Flow Metab. 26, 1479–1489. https://doi.org/10.1038/sj.jcbfm.9600303

Essa, M.M., Braidy, N., Vijayan, K.R., Subash, S., Guillemin, G.J., 2013. Excitotoxicity in the pathogenesis of autism. Neurotox. Res. 23(4), 393-400. https://doi.org/10.1007/s12640-012-9354-3

Eyre, M.D., Bartos, M., 2019. Somatostatin-Expressing Interneurons Form Axonal Projections to the Contralateral Hippocampus. Front. Neural Circuits. 13, 56. https://doi.org/10.3389/fncir.2019.00056

Feng, T., Alicea, C., Pham, V., Kirk, A., Pieraut, S., 2021. Experience-dependent inhibitory plasticity is mediated by CCK+ basket cells in the developing dentate gyrus. J. Neurosci. . 41(21), 4607-4619. 10.1523/JNEUROSCI.1207-20.2021

Flossmann, T., Kaas, T., Rahmati, V., Kiebel, S.J., Witte, O.W., Holthoff, K., Kirmse, K., 2019. Somatostatin Interneurons Promote Neuronal Synchrony in the Neonatal Hippocampus. Cell Rep. 26(12), 3173-3182.e5. https://doi.org/10.1016/j.celrep.2019.02.061

Fontes-Dutra, M., Della-Flora Nunes, G., Santos-Terra, J., Souza-Nunes, W., Bauer-Negrini, G., Hirsch, M.M., Green, L., Riesgo, R., Gottfried, C., Bambini-Junior, V., 2019. Abnormal empathy-like pro-social behaviour in the valproic acid model of autism spectrum disorder. Behav. Brain Res. 364, 11–18. https://doi.org/10.1016/J.BBR.2019.01.034

Fontes-Dutra, M., Santos-Terra, J., Deckmann, I., Schwingel, G.B., Nunes, G.D.F., Hirsch, M.M., Bauer-Negrini, G., Riesgo, R.S., Bambini-Júnior, V., Hedin-Pereira, C., Gottfried, C., 2018b. Resveratrol prevents cellular and behavioral sensory alterations in the animal model of autism induced by valproic acid. Front. Synaptic Neurosci. 10, 9. https://doi.org/10.3389/fnsyn.2018.00009

Gao, J., Wang, W.Y., Mao, Y.W., Gräff, J., Guan, J.S., Pan, L., Mak, G., Kim, D., Su, S.C., Tsai, L.H., 2010. A novel pathway regulates memory and plasticity via SIRT1 and miR-134. Nature 466, 1105–1109. https://doi.org/10.1038/nature09271

Gao, C., Yuan, X., Jiang, Z., Gan, D., Ding, L., Sun, Y., Zhou, J., Xu, L., Liu, Y., Wang, G., 2019. Regulation of AKT phosphorylation by GSK3β and PTEN to control chemoresistance in breast cancer. Breast Cancer Res. Treat. 176, 291–301. https://doi.org/10.1007/s10549-019-05239-3

Go, H.S., Kim, K.C., Choi, C.S., Jeon, S.J., Kwon, K.J., Han, S.-H., Lee, J., Cheong, J.H., Ryu, J.H., Kim, C.-H., Ko, K.H., Shin, C.Y., 2012. Prenatal exposure to valproic acid increases the neural progenitor cell pool and induces macrocephaly in rat brain via a mechanism involving the GSK-3β/β-catenin pathway. Neuropharmacology 63, 1028–1041. https://doi.org/10.1016/j.neuropharm.2012.07.028

Godavarthi, S.K., Sharma, A., Jana, N.R., 2014. Reversal of reduced parvalbumin neurons in hippocampus and amygdala of Angelman syndrome model mice by chronic

treatment of fluoxetine. J. Neurochem. 130(3), 444-454.
https://doi.org/10.1111/jnc.12726

Gogolla, N., LeBlanc, J.J., Quast, K.B., Südhof, T.C., Fagiolini, M., Hensch, T.K., 2009. Common circuit defect of excitatory-inhibitory balance in mouse models of autism. J. Neurodev. Disord. 1(2),172-181. https://doi.org/10.1007/s11689-009-9023-x

Goldfarb, E. V., Chun, M.M., Phelps, E.A., 2016. Memory-Guided Attention: Independent Contributions of the Hippocampus and Striatum. Neuron. 89(2), 317-324. https://doi.org/10.1016/j.neuron.2015.12.014

Gonçalves, J.T., Schafer, S.T., Gage, F.H., 2016. Adult Neurogenesis in the Hippocampus: From Stem Cells to Behavior. Cell. 167(4), 897-914. https://doi.org/10.1016/j.cell.2016.10.021

Gottfried, C., Bambini-Junior, V., Francis, F., Riesgo, R., Savino, W., 2015. The impact of neuroimmune alterations in autism spectrum disorder. Front. Psychiatry 6, 121. https://doi.org/10.3389/fpsyt.2015.00121

Gul, H., Marquez-Curtis, L.A., Jahroudi, N., Lo, J., Turner, A.R., Janowska-Wieczorek, A., 2009. Valproic acid increases CXCR4 expression in hematopoietic stem/progenitor cells by chromatin remodeling. Stem Cells Dev. 18, 831–838. https://doi.org/10.1089/scd.2008.0235

Harte, M.K., Powell, S.B., Swerdlow, N.R., Geyer, M.A., Reynolds, G.P., 2007. Deficits in parvalbumin and calbindin immunoreactive cells in the hippocampus of isolation reared rats. J. Neural Transm. 114(7), 893-898. https://doi.org/10.1007/s00702-007-0627-6

Hashemi, E., Ariza, J., Rogers, H., Noctor, S.C., Martínez-Cerdeño, V., 2017. The Number of Parvalbumin-Expressing Interneurons Is Decreased in the Medial Prefrontal Cortex in Autism. Cereb. Cortex 27, 1931–1943. https://doi.org/10.1093/cercor/bhw021

Hirsch, M.M., Deckmann, I., Fontes-Dutra, M., Bauer-Negrini, G., Della-Flora Nunes, G., Nunes, W., Rabelo, B., Riesgo, R., Margis, R., Bambini-Junior, V., Gottfried, C., 2018. Behavioral alterations in autism model induced by valproic acid and translational analysis of circulating microRNA. Food Chem. Toxicol. 115, 336–343. https://doi.org/10.1016/j.fct.2018.02.061

Kelsom, C., Lu, W., 2013. Development and specification of GABAergic cortical interneurons. Cell Biosci. 3(1), 19. https://doi.org/10.1186/2045-3701-3-19

Kim, J.E., Lee, D.S., Park, H., Kang, T.C., 2020. SRC/CK2/PTEN-mediated glun2b and creb dephosphorylations regulate the responsiveness to AMPA receptor antagonists in chronic epilepsy rats. Int. J. Mol. Sci. 21, 1–23. https://doi.org/10.3390/ijms21249633

Köbe, T., Witte, A.V., Schnelle, A., Tesky, V.A., Pantel, J., Schuchardt, J.P., Hahn, A., Bohlken, J., Grittner, U., Flöel, A., 2017. Impact of resveratrol on glucose control, hippocampal structure and connectivity, and memory performance in patients with mild cognitive impairment. Front. Neurosci. 11, 105. https://doi.org/10.3389/fnins.2017.00105

Kohus, Z., Káli, S., Rovira-Esteban, L., Schlingloff, D., Papp, O., Freund, T.F., Hájos, N., Gulyás, A.I., 2016. Properties and dynamics of inhibitory synaptic communication within the CA3 microcircuits of pyramidal cells and interneurons expressing parvalbumin or cholecystokinin. J. Physiol. 594(13), 3745-3774 https://doi.org/10.1113/JP272231

LaSarge, C.L., Pun, R.Y.K., Gu, Z., Santos, V.R., Danzer, S.C., 2019. Impact of mTOR hyperactive neurons on the morphology and physiology of adjacent neurons: Do PTEN KO cells make bad neighbors? Exp. Neurol. 321, 113029. https://doi.org/10.1016/j.expneurol.2019.113029

Lawrence, Y.A., Kemper, T.L., Bauman, M.L., Blatt, G.J., 2010. Parvalbumin-, calbindin-, and calretinin-immunoreactive hippocampal interneuron density in autism. Acta Neurol. Scand. 121(2), 99-108. https://doi.org/10.1111/j.1600-0404.2009.01234.x

Liu, S., Jia, J., Zhou, H., Zhang, C., Liu, L., Liu, J., Lu, L., Li, X., Kang, Y., Lou, Y., Cai, Z., Ren, Y., Kong, X., Feng, S., 2019. PTEN modulates neurites outgrowth and neuron apoptosis involving the PI3K/Akt/mTOR signaling pathway. Mol. Med. Rep. 20, 4059–4066. https://doi.org/10.3892/mmr.2019.10670

LOWRY, O.H., ROSEBROUGH, N.J., FARR, A.L., RANDALL, R.J., 1951. Protein measurement with the Folin phenol reagent. J. Biol. Chem. 193, 265–75.

Lugo, J.N., Smith, G.D., Arbuckle, E.P., White, J., Holley, A.J., Floruta, C.M., Ahmed, N., Gomez, M.C., Okonkwo, O., 2014. Deletion of PTEN produces autism-like behavioral

deficits and alterations in synaptic proteins. Front. Mol. Neurosci. 7, 27. https://doi.org/10.3389/fnmol.2014.00027

Luhmann, H.J., Fukuda, A., Kilb, W., 2015. Control of cortical neuronal migration by glutamate and GABA. Front. Cell. Neurosci. 9, 4. https://doi.org/10.3389/fncel.2015.00004

Maccaferri, G., Lacaille, J.C., 2003. Interneuron Diversity series: Hippocampal interneuron classifications - Making things as simple as possible, not simpler. Trends Neurosci. 26(10), 564-571. https://doi.org/10.1016/j.tins.2003.08.002

Maenner, M.J., Shaw, K.A., Baio, J., Washington, A., Patrick, M., DiRienzo, M., Christensen, D.L., Wiggins, L.D., Pettygrove, S., Andrews, J.G., Lopez, M., Hudson, A., Baroud, T., Schwenk, Y., White, T., Rosenberg, C.R., Lee, L.C., Harrington, R.A., Huston, M., Hewitt, A., Esler, A., Hall-Lande, J., Poynter, J.N., Hallas-Muchow, L., Constantino, J.N., Fitzgerald, R.T., Zahorodny, W., Shenouda, J., Daniels, J.L., Warren, Z., Vehorn, A., Salinas, A., Durkin, M.S., Dietz, P.M., 2020. Prevalence of autism spectrum disorder among children aged 8 Years-Autism and developmental disabilities monitoring network, 11 Sites, United States, 2016. MMWR Surveill. Summ. 63(2), 1-21. https://doi.org/10.15585/MMWR.SS6904A1

Maglóczky, Z.S., Wittner, L., Borhegyi, Z.S., Halász, P., Vajda, J., Czirják, S., Freund, T.F., 2000. Changes in the distribution and connectivity of interneurons in the epileptic human dentate gyrus. Neuroscience 96(1), 7-25. https://doi.org/10.1016/S0306-4522(99)00474-1

Manent, J.B., Jorquera, I., Ben-Ari, Y., Aniksztejn, L., Represa, A., 2006. Glutamate acting on AMPA but not NMDA receptors modulates the migration of hippocampal interneurons. J. Neurosci. 26(22), 5901-5909. https://doi.org/10.1523/JNEUROSCI.1033-06.2006

Marín, O., Rubenstein, J.L.R., 2003. Cell migration in the forebrain. Annu. Rev. Neurosci. 26, 441–83. https://doi.org/10.1146/annurev.neuro.26.041002.131058

Meyer, U., Nyffeler, M., Yee, B.K., Knuesel, I., Feldon, J., 2008. Adult brain and behavioral pathological markers of prenatal immune challenge during early/middle and late fetal development in mice. Brain. Behav. Immun. 22, 469–486. https://doi.org/10.1016/j.bbi.2007.09.012

Murray, A.J., Sauer, J.F., Riedel, G., McClure, C., Ansel, L., Cheyne, L., Bartos, M., Wisden, W., Wulff, P., 2011. Parvalbumin-positive CA1 interneurons are required for spatial working but not for reference memory. Nat. Neurosci. 14(3), 297-299. https://doi.org/10.1038/nn.2751

Nelson, S.B., Valakh, V., 2015. Excitatory/Inhibitory Balance and Circuit Homeostasis in Autism Spectrum Disorders. Neuron. 87(4), 684-698. https://doi.org/10.1016/j.neuron.2015.07.033

Nicolini, C., Ahn, Y., Michalski, B., Rho, J.M., Fahnestock, M., 2015. Decreased mTOR signaling pathway in human idiopathic autism and in rats exposed to valproic acid. Acta Neuropathol. Commun. 3, 3. https://doi.org/10.1186/s40478-015-0184-4

Ognjanovski, N., Schaeffer, S., Wu, J., Mofakham, S., Maruyama, D., Zochowski, M., Aton, S.J., 2017. Parvalbumin-expressing interneurons coordinate hippocampal network dynamics required for memory consolidation. Nat. Commun. 8, 15039. https://doi.org/10.1038/ncomms15039

Olloquequi, J., Cornejo-Córdova, E., Verdaguer, E., Soriano, F.X., Binvignat, O., Auladell, C., Camins, A., 2018. Excitotoxicity in the pathogenesis of neurological and psychiatric disorders: Therapeutic implications. J. Psychopharmacol. 32(3), 265-275. https://doi.org/10.1177/0269881118754680

Pauli, E., Hildebrandt, M., Romstöck, J., Stefan, H., Blümcke, I., 2006. Deficient memory acquisition in temporal lobe epilepsy is predicted by hippocampal granule cell loss. Neurology 67(8), 1383-1389. https://doi.org/10.1212/01.wnl.0000239828.36651.73

Pelkey, K.A., Chittajallu, R., Craig, M.T., Tricoire, L., Wester, J.C., McBain, C.J., 2017. Hippocampal gabaergic inhibitory interneurons. Physiol. Rev. 97(4), 1619-1747 https://doi.org/10.1152/physrev.00007.2017

Plitman, E., Nakajima, S., de la Fuente-Sandoval, C., Gerretsen, P., Chakravarty, M.M., Kobylianskii, J., Chung, J.K., Caravaggio, F., Iwata, Y., Remington, G., Graff-Guerrero, A., 2014. Glutamate-mediated excitotoxicity in schizophrenia: A review. Eur. Neuropsychopharmacol. 24(10), 1591-1605. https://doi.org/10.1016/j.euroneuro.2014.07.015

Qin, X., Zaki, M.G., Chen, Z., Jakova, E., Ming, Z., Cayabyab, F.S., 2021. Adenosine

Signaling and Clathrin-Mediated Endocytosis of Glutamate AMPA Receptors in Delayed Hypoxic Injury in Rat Hippocampus: Role of Casein Kinase 2. Mol. Neurobiol. 58, 1932–1951. https://doi.org/10.1007/s12035-020-02246-0

Rubin, R.D., Watson, P.D., Duff, M.C., Cohen, N.J., 2014. The role of the hippocampus in flexible cognition and social behavior. Front. Hum. Neurosci. 8, 742. https://doi.org/10.3389/fnhum.2014.00742

Santos, V.R., Pun, R.Y.K., Arafa, S.R., LaSarge, C.L., Rowley, S., Khademi, S., Bouley, T., Holland, K.D., Garcia-Cairasco, N., Danzer, S.C., 2017. PTEN deletion increases hippocampal granule cell excitability in male and female mice. Neurobiol. Dis. 108, 339–351. https://doi.org/10.1016/j.nbd.2017.08.014

Sohal, V.S., Rubenstein, J.L.R., 2019. Excitation-inhibition balance as a framework for investigating mechanisms in neuropsychiatric disorders. Mol. Psychiatry 24, 1248. https://doi.org/10.1038/S41380-019-0426-0

Shin, S., Santi, A., Huang, S., 2021. Conditional Pten knockout in parvalbumin- or somatostatin-positive neurons sufficiently leads to autism-related behavioral phenotypes. Mol. Brain. 14, 24. https://doi.org/10.1186/s13041-021-00731-8

Sik, A., Tamamaki, N., Freund, T.F., 1993. Complete Axon Arborization of a Single CA3 Pyramidal Cell in the Rat Hippocampus, and its Relationship With Postsynaptic Parvalbumin- containing Interneurons. Eur. J. Neurosci. 5(12), 1719-1728. https://doi.org/10.1111/j.1460-9568.1993.tb00239.x

Skelton, P.D., Frazel, P.W., Lee, D., Suh, H., Luikart, B.W., 2019. Pten loss results in inappropriate excitatory connectivity. Mol. Psychiatry 24, 1627–1640. https://doi.org/10.1038/s41380-019-0412-6

Smith, A.L., Jung, E.M., Jeon, B.T., Kim, W.Y., 2020. Arid1b haploinsufficiency in parvalbumin- or somatostatin-expressing interneurons leads to distinct ASD-like and ID-like behavior. Sci. Rep. 10, 7834. https://doi.org/10.1038/s41598-020-64066-5

Sohal, V.S., Rubenstein, J.L.R., 2019. Excitation-inhibition balance as a framework for investigating mechanisms in neuropsychiatric disorders. Mol. Psychiatry 24, 1248. https://doi.org/10.1038/S41380-019-0426-0

Sullivan, D., Csicsvari, J., Mizuseki, K., Montgomery, S., Diba, K., Buzsáki, G., 2011.

Relationships between hippocampal sharp waves, ripples, and fast gamma oscillation: Influence of dentate and entorhinal cortical activity. J. Neurosci. 31(23), 8605-8616 https://doi.org/10.1523/JNEUROSCI.0294-11.2011

Tai, C., Abe, Y., Westenbroek, R.E., Scheuer, T., Catterall, W.A., 2014. Impaired excitability of somatostatin- and parvalbumin-expressing cortical interneurons in a mouse model of Dravet syndrome. Proc. Natl. Acad. Sci. 111, E3139–E3148. https://doi.org/10.1073/pnas.1411131111

Tai, C., Abe, Y., Westenbroek, R.E., Scheuer, T., Catterall, W.A., 2014. Impaired excitability of somatostatin- and parvalbumin-expressing cortical interneurons in a mouse model of Dravet syndrome. Proc. Natl. Acad. Sci. U. S. A. 111(30), E3139-E3148 https://doi.org/10.1073/pnas.1411131111

Tallent, M.K., 2007. Somatostatin in the dentate gyrus. 163, 265-284. Prog. Brain Res. https://doi.org/10.1016/S0079-6123(07)63016-7

Tavitian, A., Song, W., Schipper, H.M., 2019. Dentate Gyrus Immaturity in Schizophrenia. Neuroscientist. 25(6), 528-547. https://doi.org/10.1177/1073858418824072

Thom, M., 2014. Review: Hippocampal sclerosis in epilepsy: A neuropathology review. Neuropathol. Appl. Neurobiol. 40(5), 520-543. https://doi.org/10.1111/nan.12150

Vogt, D., Cho, K.K.A., Lee, A.T., Sohal, V.S., Rubenstein, J.L.R., 2015. The Parvalbumin/Somatostatin Ratio Is Increased in Pten Mutant Mice and by Human PTEN ASD Alleles. Cell Rep. 11, 944–956. https://doi.org/10.1016/j.celrep.2015.04.019

Wang, S.J., Zhao, X.H., Chen, W., Bo, N., Wang, X.J., Chi, Z.F., Wu, W., 2015. Sirtuin 1 activation enhances the PGC-1á/mitochondrial antioxidant system pathway in status epilepticus. Mol. Med. Rep. 11, 521–526. https://doi.org/10.3892/mmr.2014.2724

Wei, Y., Han, X., Zhao, C., 2020. PDK1 regulates the survival of the developing cortical interneurons. Mol. Brain. 13, 65. https://doi.org/10.1186/s13041-020-00604-6

Wöhr, M., Orduz, D., Gregory, P., Moreno, H., Khan, U., Vörckel, K.J., Wolfer, D.P., Welzl, H., Gall, D., Schiffmann, S.N., Schwaller, B., 2015. Lack of parvalbumin in mice leads to behavioral deficits relevant to all human autism core symptoms and related neural morphofunctional abnormalities. Transl. Psychiatry. 5, e525. https://doi.org/10.1038/tp.2015.19

Wu, H.-F., Chen, P.S., Chen, Y.-J., Lee, C.-W., Chen, I.-T., Lin, H.-C., 2017. Alleviation of N-Methyl-d-Aspartate Receptor-Dependent Long-Term Depression via Regulation of the Glycogen Synthase Kinase-3β Pathway in the Amygdala of a Valproic Acid-Induced Animal Model of Autism. Mol. Neurobiol. 54, 5264–5276. https://doi.org/10.1007/s12035-016-0074-1

Xing, X., Zhang, J., Wu, K., Cao, B., Li, X., Jiang, F., Hu, Z., Xia, K., Li, J. Da, 2019. Suppression of Akt-mTOR pathway rescued the social behavior in Cntnap2-deficient mice. Sci. Rep. 9, 3041. https://doi.org/10.1038/s41598-019-39434-5

Yuan, M., Meyer, T., Benkowitz, C., Savanthrapadian, S., Ansel-Bollepalli, L., Foggetti, A., Wulff, P., Alcami, P., Elgueta, C., Bartos, M., 2017. Somatostatin-positive interneurons in the dentate gyrus of mice provide local- and long-range septal synaptic inhibition. Elife. 6, e21105. https://doi.org/10.7554/elife.21105

List of Figures

Figure 1: Prenatal exposure to VPA induced morphological changes in the hippocampus (HC) of P120 animals. A) Illustrative images of HC and subregions. B) Representative images of immunofluorescence of the total HC labelling NeuN (red). C) Representative images of DG, arrows point to the main region where VPA induced neuronal loss (demonstrated with dashed lines in the other groups). D) Representative images of CA1, the arrow points to the loss of compaction observed in the VPA group (the width lines highlight the difference observed in the VPA group). Coordinates: bregma: -2.92 mm, interaural: 6.08 mm, - bregma: -3.24 mm, interaural: 5.76 mm. Scale bar B: 250 µm, Scale Bar C, D: 50 µm. C(Control)=4, R(RSV)=4, V(VPA)=4, R+V(RSV+VPA)=3.

Figure 2: Prenatal exposure to VPA decreased the number of total neurons per area in the dentate gyrus of P120 animals. Values presented as Mean ± SD. Statistical analysis: two-way ANOVA followed by Bonferroni post-test. CON=4, RSV=4, VPA=4, RSV+VPA=3. Symbols indicate significant differences in the post test, when the interaction was significative (#: VPA-CON; *: VPA-RSV, and $: RSV+VPA-VPA $p<0.05$). Complete statistics were summarized in Supplementary Table 1. Factors were applied to avoid decimal numbers in the Y axis.

Figure 3: Representative images of immunofluorescence in the dentate gyrus. A) Cb, calbindin (green); NeuN (red); DAPI (blue), B) Pv, parvalbumin (green); NeuN (red); DAPI
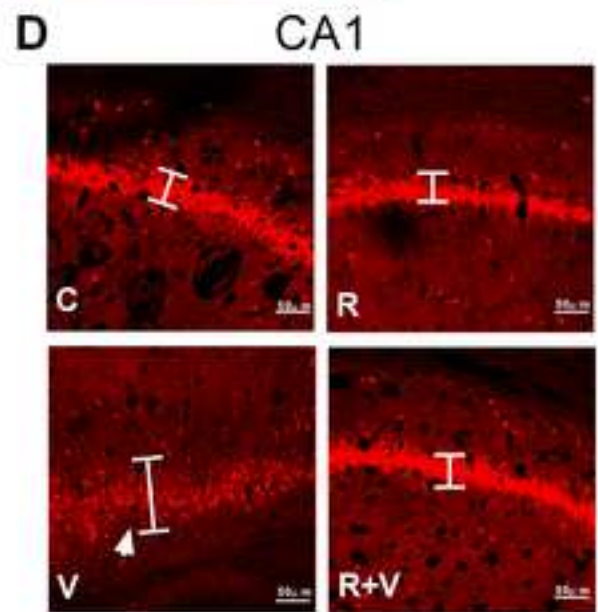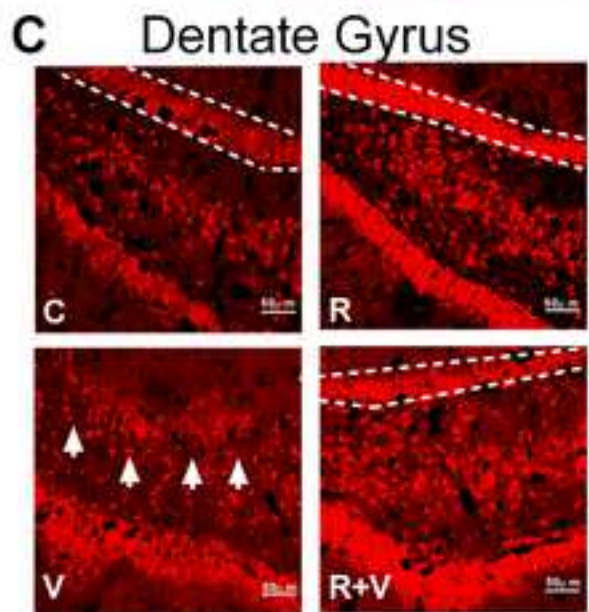
(blue), C) Som, somatostatin (red); NeuN (green); DAPI (blue). A representative interneuron was highlighted in a box in the top corner (scale bar: 10 μm). CON=4, RSV=4, VPA=4, RSV+VPA=3. Scale bar: 50 μm. Arrowheads indicate the respective interneurons. RSV prevented CB^+ reduction induced by VPA in number (A1), no differences were found for ratio (A2). No differences among groups were observed for PV^+ number (B1) and ratio (B2). VPA increased the SOM^+ number (C1) and the preventive effect of RSV was observed in SOM^+ ratio (C2). Symbols indicate significant differences in the post test, when interaction was significative (#: VPA-CON; *: VPA-RSV, and $: RSV+VPA-VPA $p<0.05$). When significant differences appeared only in separated factors, the difference was represented by lines indicating $p<0.05$. Statistical analysis: two-way ANOVA followed by Bonferroni post-test. Data demonstrated as mean ± SD. Complete statistics were summarized in Supplementary Tables 2, 3, and 4. The high density of cellular nuclei (stained blue) and neuronal bodies (especially in the assays where NeuN is marked with red) in some regions result in a violet/purple color. C: Control; R: RSV; V: VPA; R+V: RSV+VPA. Factors were applied to avoid decimal numbers in the Y axis.

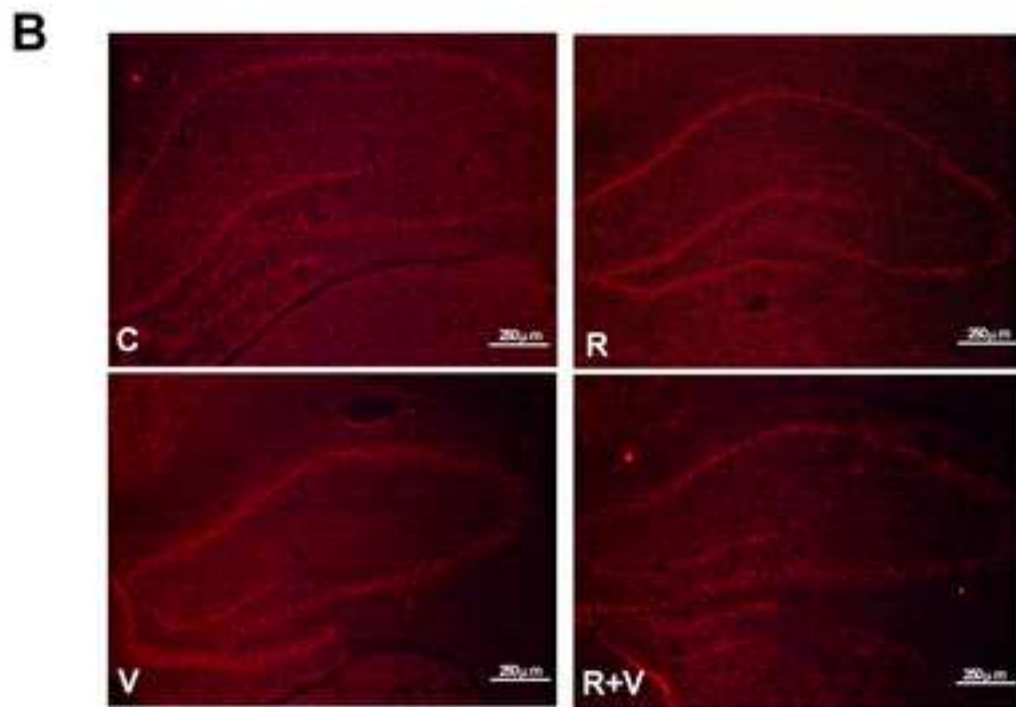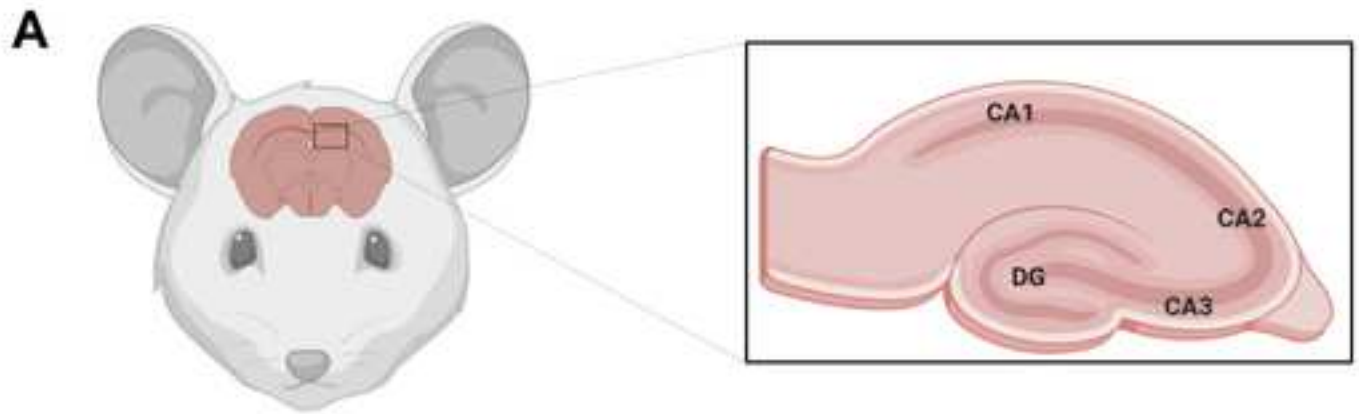**Figure 4: Representative images of immunofluorescence in CA1**. A) Cb, calbindin (green); NeuN (red); DAPI (blue). B) Pv, parvalbumin (green); NeuN (red); DAPI (blue), C) Som, somatostatin (red); NeuN (green); DAPI (blue). A representative interneuron was highlighted in a box in the top corner (scale bar: 10 μm). CON=4, RSV=4, VPA=4, RSV+VPA=3. Scale bar: 50 μm. Arrowheads indicate the respective interneurons. RSV prevented the reduction in CB^+ number (A1) and ratio (A2) induced by VPA. VPA induced reduction in PV^+ number, not prevented by RSV (B1) and no differences were found for PV^+ ratio (B2). VPA and RSV induced reduction in SOM^+ number (C1) and no differences were found for ratio (C2). Symbols indicate significant differences in the post test, when interaction was significative (#: VPA-CON; *: VPA-RSV, and $: RSV+VPA-VPA $p<0.05$). When significant differences appeared only in separated factors, the difference was represented by lines indicating $p<0.05$. Statistical analysis: two-way ANOVA followed by Bonferroni post-test. Data demonstrated as mean ± SD. Complete statistics were summarized in Supplementary Tables 2, 3, and 4. The high density of cellular nuclei (stained blue) and neuronal bodies (especially in the assays where NeuN is marked with red) in some regions result in a violet/purple color. C: Control; R: RSV; V: VPA; R+V: RSV+VPA. Factors were applied to avoid decimal numbers in the Y axis.
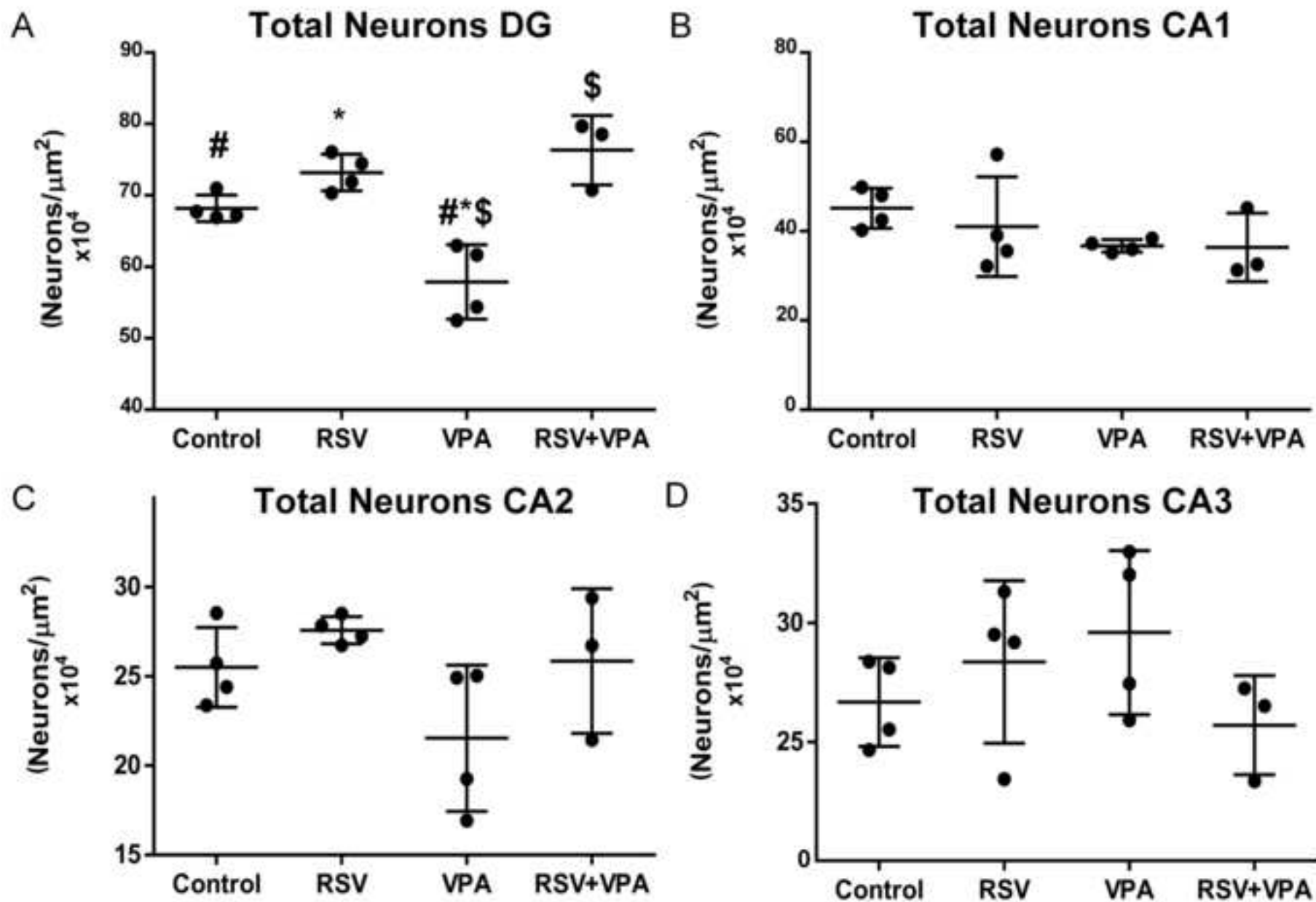
Figure 5: Representative images of immunofluorescence in CA2. A) Cb, calbindin (green); NeuN (red); DAPI (blue). B) Pv, parvalbumin (green); NeuN (red); DAPI (blue), C)

Som, somatostatin (red); NeuN (green); DAPI (blue). A representative interneuron was highlighted in a box in the top corner (scale bar: 10 μm). CON=4, RSV=4, VPA=4, RSV+VPA=3. Scale bar: 50 μm. Arrowheads indicate the respective interneurons. No differences were found in CB$^+$ number (A1) and ratio (A2). No differences were found in PV$^+$ number (B1) ratio (B2). VPA induced reduction in SOM$^+$ number (C1) and RSV prevented reduction in SOM$^+$ ratio induced by VPA (C2). Symbols indicate significant differences in the post test, when interaction was significative (#: VPA-CON; *: VPA-RSV, and $: RSV+VPA-VPA $p<0.05$). When significant differences appeared only in separated factors, the difference was represented by lines indicating $p<0.05$. Statistical analysis: two-way ANOVA followed by Bonferroni post-test. Data demonstrated as mean ± SD. Complete statistics were summarized in Supplementary Tables 2, 3, and 4. The high density of cellular nuclei (stained blue) and neuronal bodies (especially in the assays where NeuN is marked with red) in some regions result in a violet/purple color. C: Control; R: RSV; V: VPA; R+V: RSV+VPA. Factors were applied to avoid decimal numbers in the Y axis.
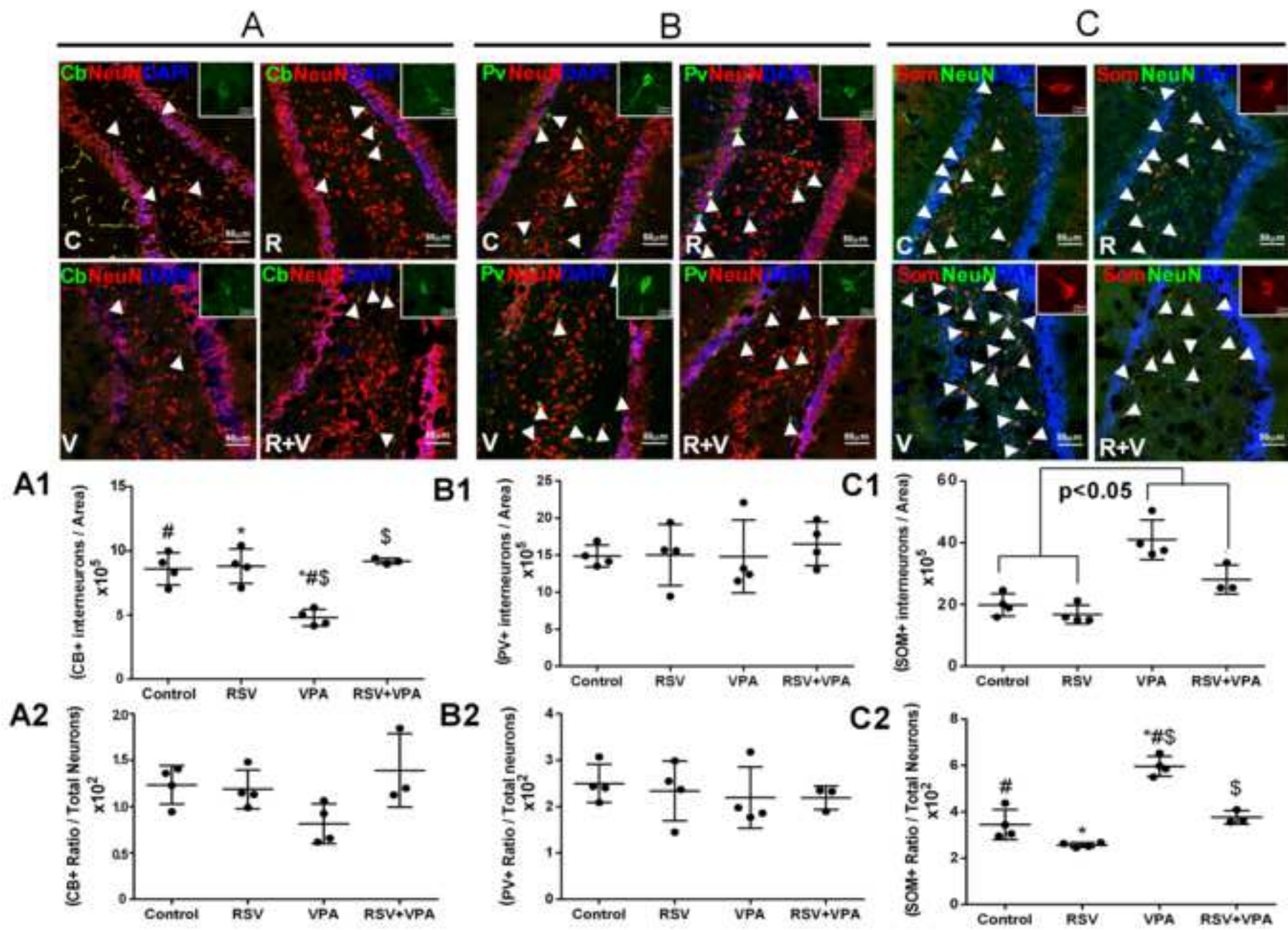
Figure 6: Representative images of immunofluorescence in CA3. A) Cb, calbindin (green); NeuN (red); DAPI (blue). B) Pv, parvalbumin (green); NeuN (red); DAPI (blue), C) Som, somatostatin (red); NeuN (green); DAPI (blue). A representative interneuron was highlighted in a box in the top corner (scale bar: 10 μm). CON=4, RSV=4, VPA=4, RSV+VPA=3. Scale bar: 50 μm. Arrowheads indicate the respective interneurons. No differences were found in CB$^+$ number (A1) and ratio (A2). VPA induced reduction in PV$^+$ number (B1) and ratio (B2), without RSV prevention. No differences were found in SOM$^+$ number (C1) and ratio (C2). Symbols indicate significant differences in the post test, when interaction was significative (#: VPA-CON; *: VPA-RSV, and $: RSV+VPA-VPA $p<0.05$). When significant differences appeared only in separated factors, the difference was represented by lines indicating $p<0.05$. Statistical analysis: two-way ANOVA followed by Bonferroni post-test. Data demonstrated as mean ± SD. Complete statistics were summarized in Supplementary Tables 2, 3, and 4. The high density of cellular nuclei (stained blue) and neuronal bodies (especially in the assays where NeuN is marked with red) in some regions result in a violet/purple color. C: Control; R: RSV; V: VPA; R+V: RSV+VPA. Factors were applied to avoid decimal numbers in the Y axis.

Figure 7. Prenatal exposure to VPA induced changes in the immunocontent of Akt, PTEN, and CK2 in the hippocampus of adult animals. Prenatal exposure to VPA decreased the immunocontent of A) PTEN, B) Akt and increased C) CK2, without altering the content of D) GSK3β. No differences were found for phosphorylation levels
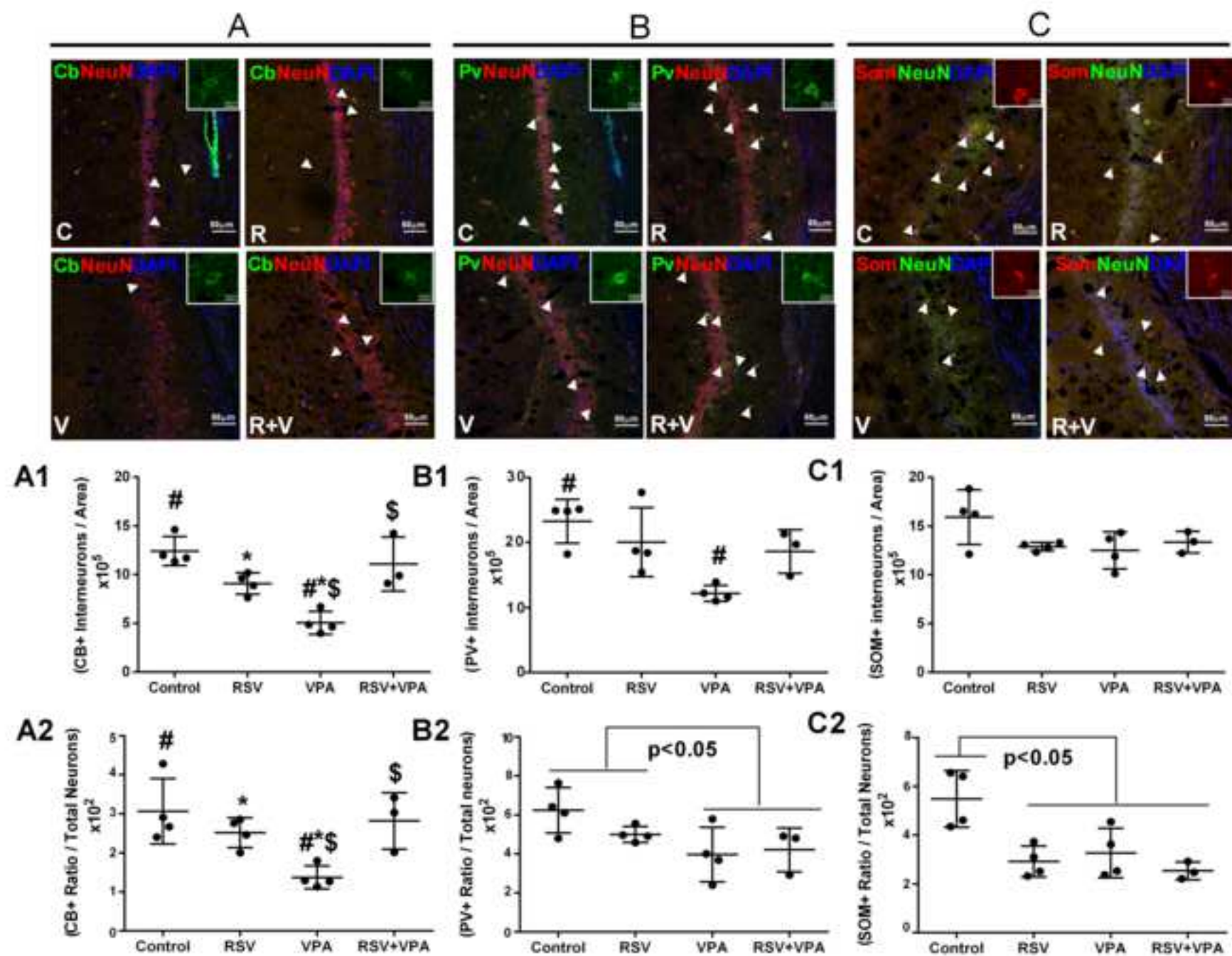
(Supplementary Table 5). When significant differences appeared only in separated factors, the difference was represented by lines indicating p<0.05. Values presented as Mean ± SD. Statistical analysis: two-way ANOVA followed by Bonferroni post-test. CON=6, RSV=6, VPA=6, RSV+VPA=6. *p <0.05. The immunocontent of PTEN (54 kDa), AKT (60 kDa), CK2 (42 kDa) and GSK3β (46 kDa) was normalized by the β-actin (42 kDa) loading control.
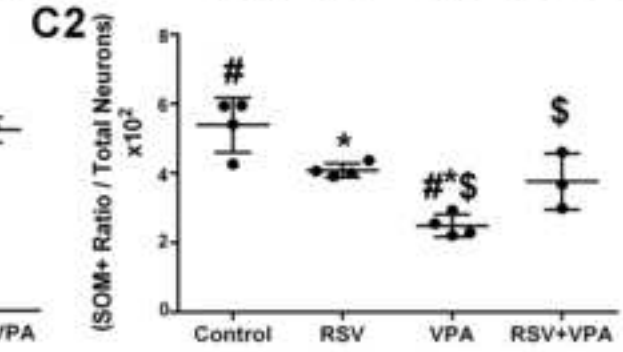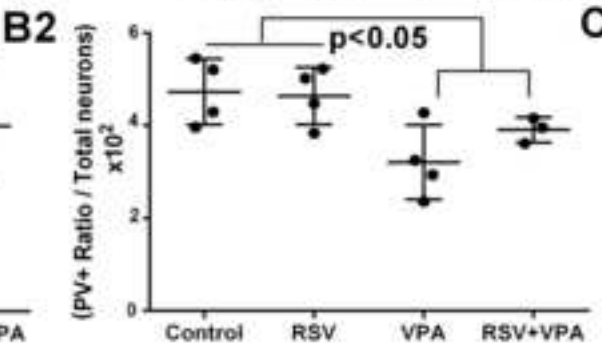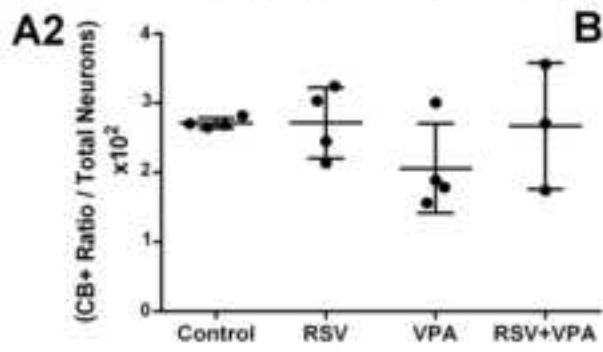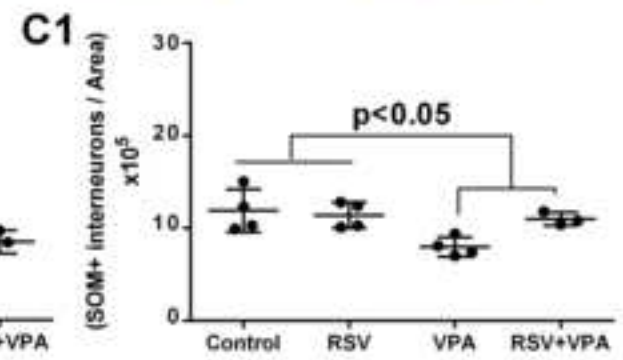
Figure 2

Figure 2

Figure 3

Figure 4

Click here to access/download;Figure;Figure 4.tif

Figure 4

Figure 5

Click here to access/download;Figure;Figure 5.tif

Figure 6

Figure 7

Click here to access/download;Figure;Figure 7.tif ⬇

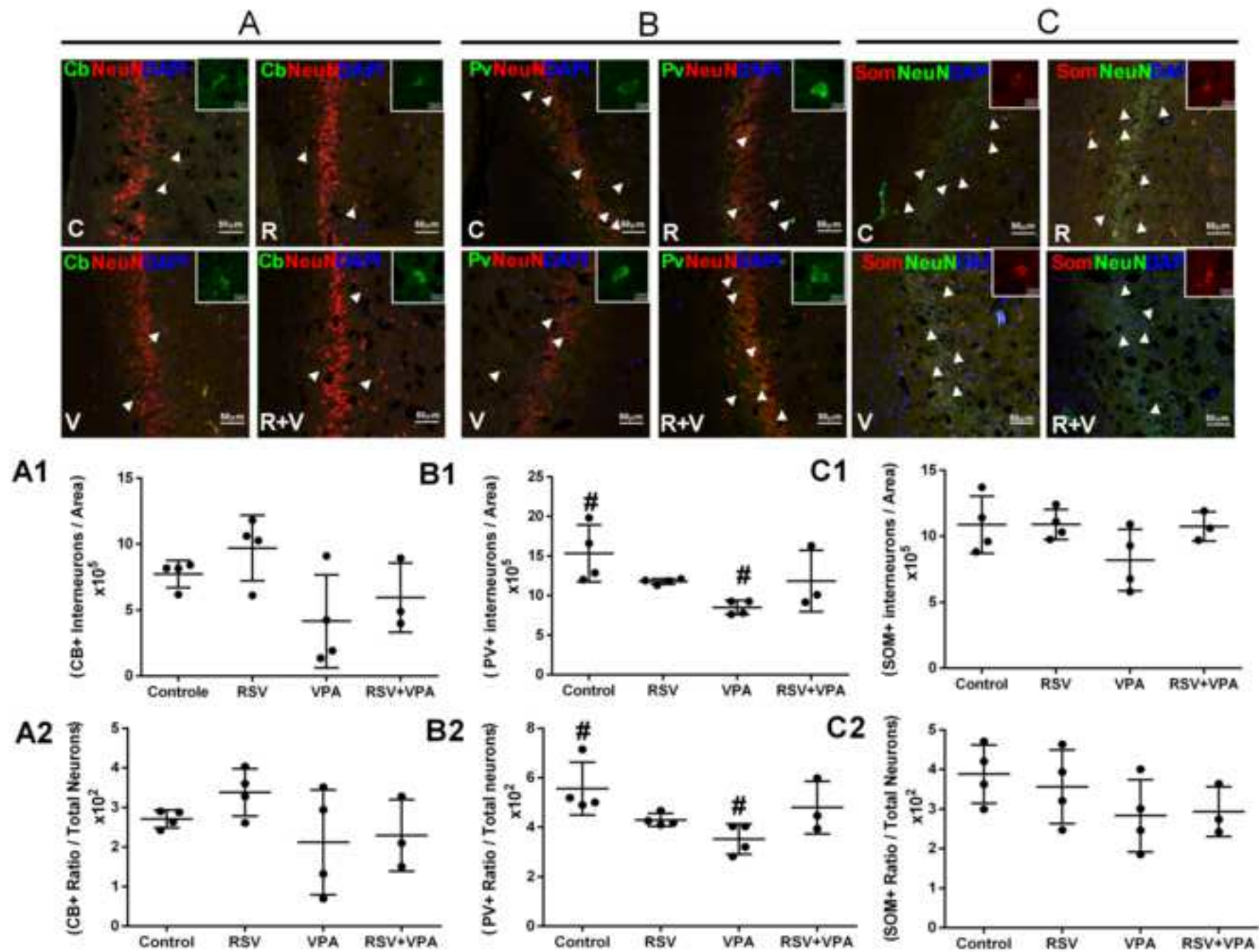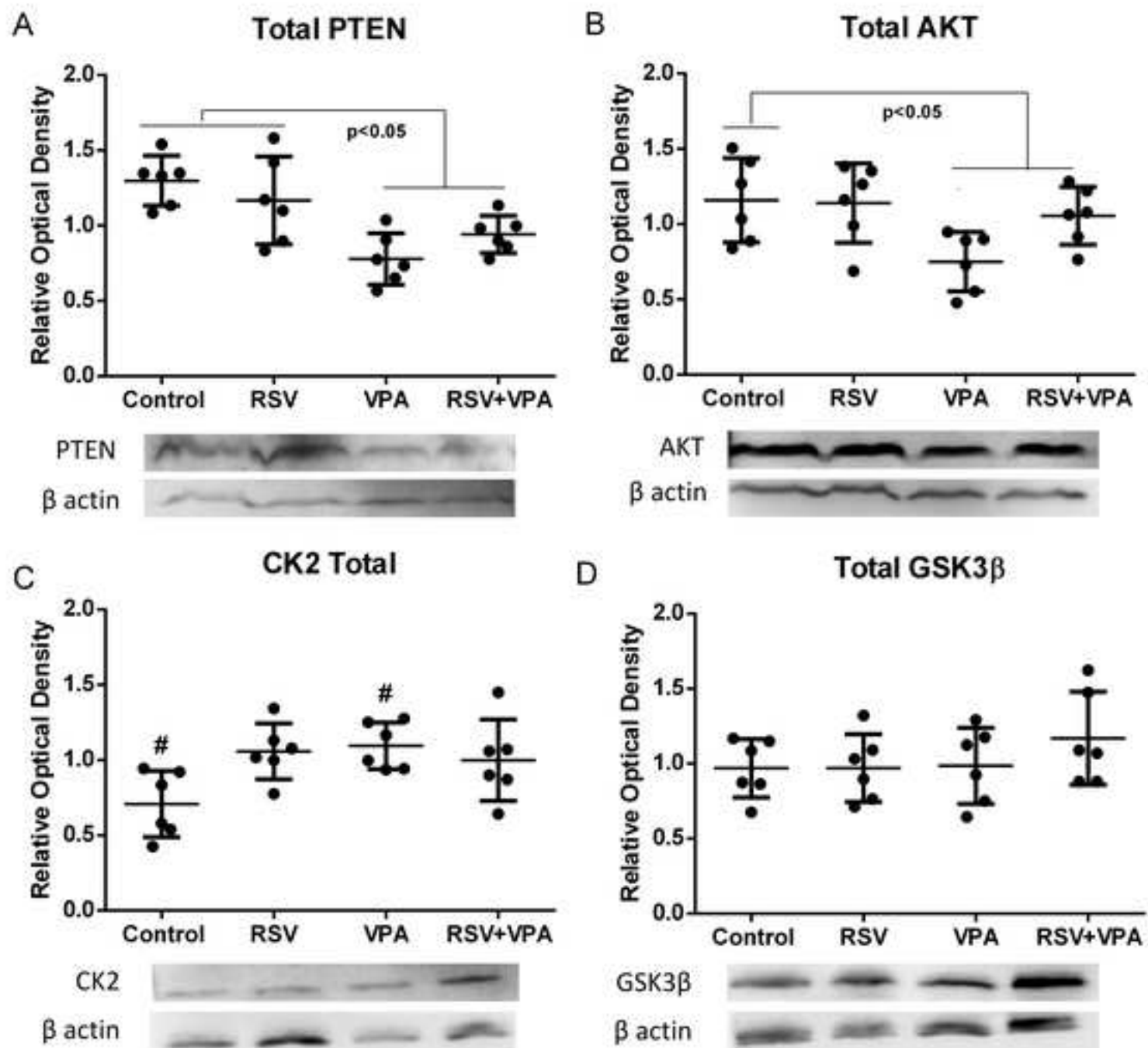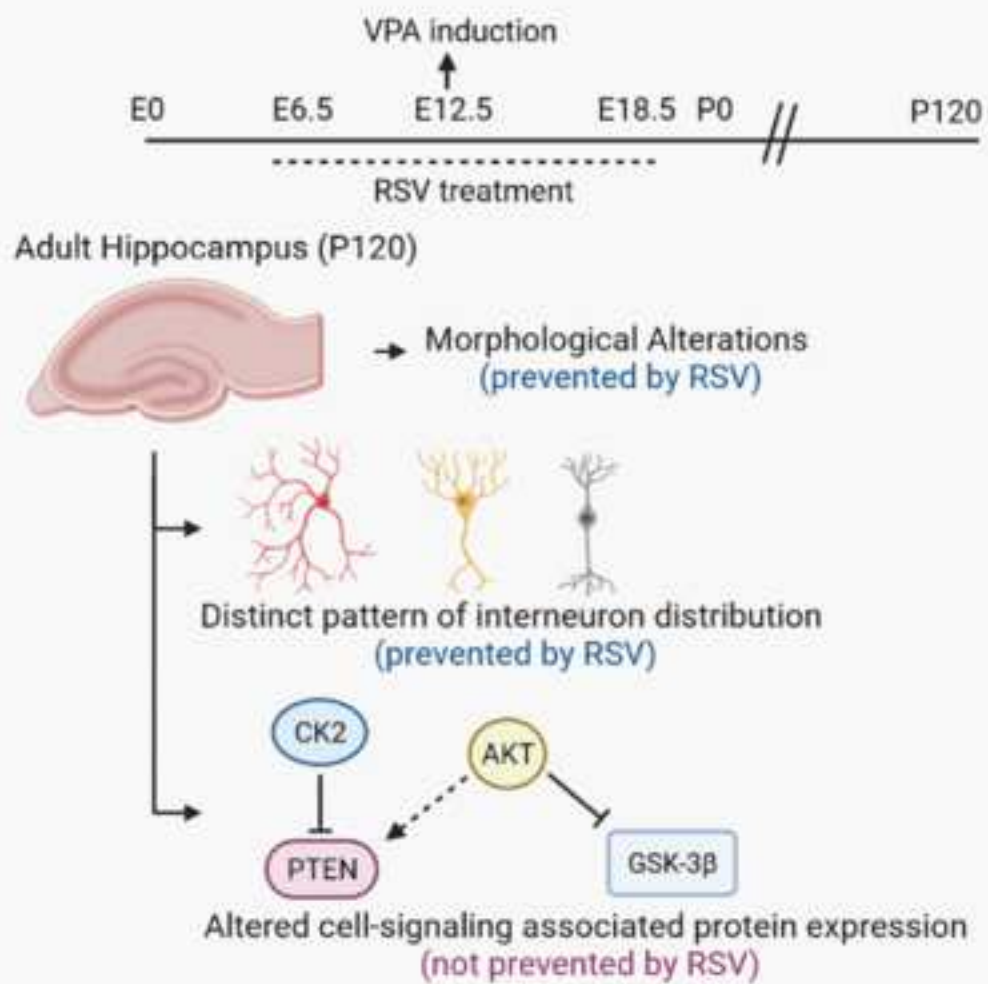**A** Total PTEN

B Total AKT

C CK2 Total

D Total GSK3β
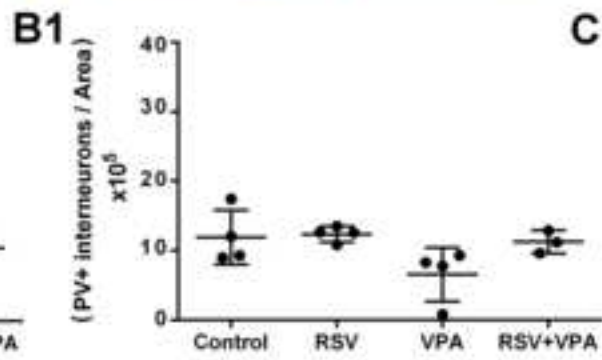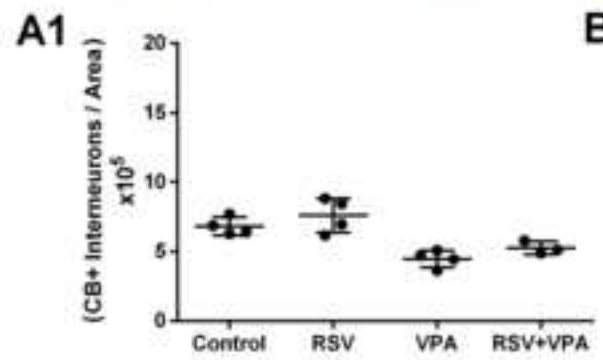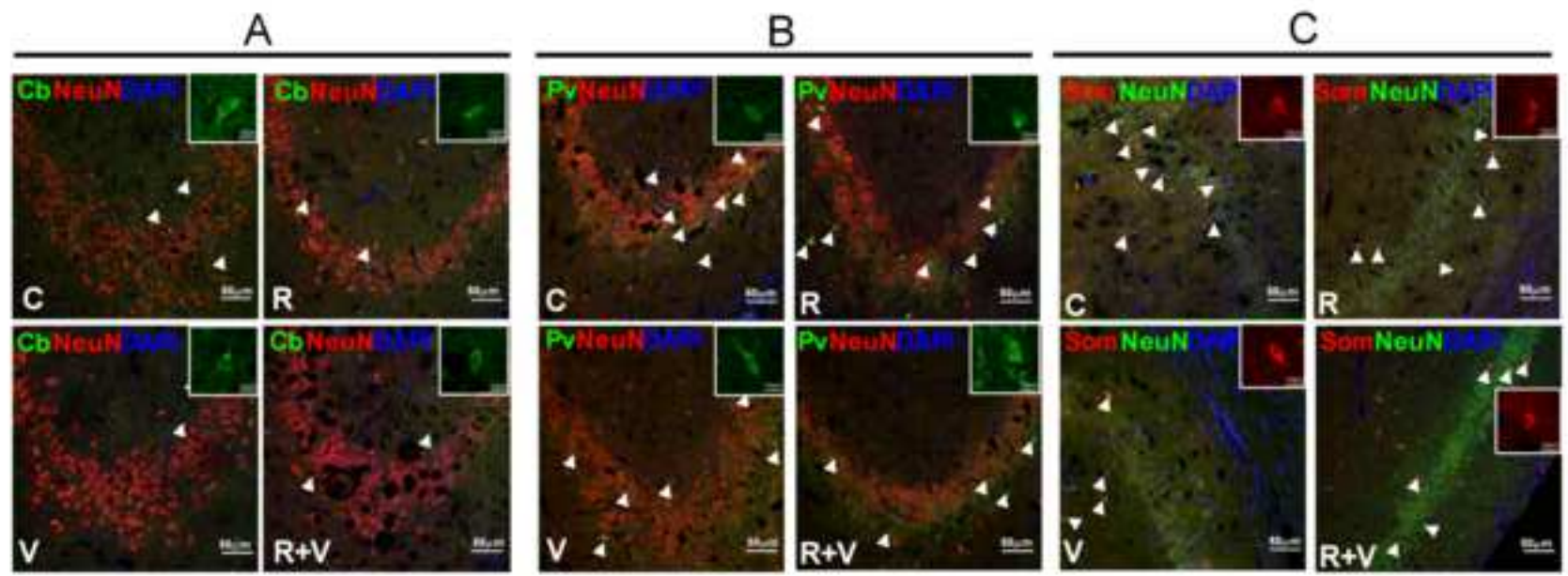
Click here to access/download
Electronic Supplementary Material (online publication only)
Santos-Terra et al., 2021_ supplementary.docx

CREDIT AUTHOR STATEMENT:

Júlio Santos-Terra: Conceptualization, methodology, validation, formal analysis, investigation, writing - original draft preparation, writing - review and editing preparation, project administration. **Iohanna Deckmann:** Conceptualization, methodology, validation, investigation, writing - review and editing preparation. **Gustavo Brum Schwingel:** Conceptualization, methodology, validation, investigation. **André Vinícius Contri Paz:** Conceptualization, methodology, validation, investigation. **Clarissa S. Gama:** Conceptualization, resources, funding acquisition. **Victorio Bambini-Junior:** Conceptualization, methodology, resources, writing - review and editing preparation, funding acquisition. **Mellanie Fontes-Dutra:** Conceptualization, methodology, validation, investigation, writing - review and editing preparation. **Carmem Gottfried:** Conceptualization, methodology, resources, writing - review and editing preparation, supervision, funding acquisition.